Studies Related to Analysis of Seepage of Sea Water through the Dyke and from underneath the Flood Regulator

as part of

Development of Detailed Project Report of Kalpasar Dam Project

being undertaken by the

National Centre for Coastal Research, Ministry of Earth Sciences

Department of Civil Engineering

Indian Institute of Technology Delhi

New Delhi

December 2023

Table of Contents

Project Team

Investigators

- G. V. Ramana, Professor, Dept. of Civil Engineering, IIT Delhi
- Sourabh Mhaski, PMRF Research Scholar, Dept. of Civil Engineering, IIT Delhi

Acknowledgements

- NCCR team for providing the necessary cross-sections in digital form, material properties, tidal variations, and freshwater reservoir variations.
- PMC for providing technical inputs.

List of Tables

16	Total quantity of water (m^3/m) flowing through embankment and foundation in 1 year at flood regulator section
17	Total quantity of salt mass (kg/m) transported through embankment and foundation in 1 year at -30 m section
18	Total quantity of salt mass (kg/m) transported through embankment and foundation in 1 year at -25 m section
19	Total quantity of salt mass (kg/m) transported through embankment and foundation in 1 year at -20 m section
20	Total quantity of salt mass (kg/m) transported through embankment and foundation in 1 year at -15 m section
21	Total quantity of salt mass (kg/m) transported through embankment and foundation in 1 year at -10 m (with caisson) section
22	Total quantity of salt mass (kg/m) transported through embankment and foundation in 1 year at -10 m (without caisson) section
23	Total quantity of salt mass (kg/m) transported through embankment and foundation in 1 year at -5 m section
24	Total quantity of salt mass (kg/m) transported through embankment and foundation in 1 year at 0 m section
25	Total quantity of salt mass (kg/m) transported through embankment and foundation in 1 year at +2 m section
26	Total quantity of salt mass (kg/m) transported through embankment and foundation in 1 year at +5 m section
27	Total quantity of salt mass (kg/m) transported through embankment and foundation in 1 year at flood regulator section

List of Figures

1. Background

The Kalpasar Department, Government of Gujarat, proposes to construct world's biggest artificial freshwater reservoir in Gulf of Khambhat region, Gujarat, India. The Gulf of Khambhat Development Project (Kalpasar) is a multipurpose mega project comprising the construction of a dam for a length of about 60 km out of which 30 km in gulf and balance 30 km length is extended on both flanks upto nearest road crossing between Bhavnagar on western coast and village Paniadara in Bharuch District on eastern coast of Gulf of Khambhat. This dam is contemplated to meet the increasing demands of water supply for irrigation, drinking, and industrial needs as well as to facilitate rail and road transport, land reclamation, etc.

A proposal for carrying out the seepage analysis of seawater and quantification of salt mass influx through the dyke and from underneath the flood regulator under varying reservoir conditions and tidal variations was given by IIT Delhi in October 2022 and was approved by NCCR through F. No. MOES/NCCR/62/Kalpasar/SA/2022 (Dated: 02/12/2022).

2. Scope of work

2.1 Seepage analysis of dyke

- Review of cross-sections of dyke and identifying the critical typical cross-sections.
- Modelling seepage through the dyke at all identified critical typical cross-sections for various water levels in reservoir and tidal cycles in open sea, considering transients of rising and falling levels of water on the two faces of the dyke.
- Estimation of total seepage quantity of salt water into the reservoir for various water level scenarios in a year.
- Suggestions on suitable geotechnical measures for reducing the seepage through the dyke.

2.2 Seepage analysis of flood regulator

- Review of cross-sections of flood regulator.
- Modelling seepage through flood regulator for various water levels in reservoir and tidal cycles in open sea, considering transients of rising and falling levels of water on the two sides of the flood regulator.

- Estimation of total seepage quantity of salt water into the reservoir for various scenarios in a year.
- Optimizing the depth of upstream and downstream cutoff walls underneath the flood regulator.

3. Methodology

3.1 Mathematical model

The soil is assumed to be a three-phase medium, with the pores (voids) filled with water and air. Additionally, salt (solute) is dissolved in the water phase. Essential parameters required for the development of the coupled flow-solute transport model are defined as follows,

- Salt mass fraction/salinity ω: mass of dissolved salt per unit mass of water.
- For seawater, $\omega_s = 35000$ ppm = 35 gm/L = 35 kg/m^3.
- Normalized mass fraction $C = \omega/\omega_s$ (0 for freshwater and 1 for seawater).

The density of water (ρ_f) varies as a function of the dissolved salt concentration and is given by,

$$\rho_f = \rho_{f0} + (\rho_s - \rho_{f0})C \tag{1}$$

where ρ_{f0} = 1000 kg/m^3 and ρ_s = 1025 kg/m^3 are the density of the freshwater and seawater, respectively. The dissolved salt is transported by the following mechanisms [1],

- Advection: salt transport due to flow of water.
- Mechanical dispersion: spreading of the salt due to water flowing through the soil pores.
- Molecular diffusion: spreading of the salt due to concentration gradient.

Mechanical dispersion and molecular diffusion are simultaneous processes and are collectively referred to as hydrodynamic dispersion. The fundamental governing equations for the coupled groundwater flow and salt transport are developed using the mass and linear momentum conservation for the water phase and dissolved salt, and are given as follows:

Flow model,

$$\frac{\partial h_p}{\partial t} = \frac{1}{\tilde{C}_{sr}}\nabla.\left(\frac{k_f \delta_c}{\mu_r}\left(\nabla h_p + \delta_c \nabla y\right)\right) + \frac{\beta_c}{\tilde{C}_{sr}}\nabla.\left(n_f \boldsymbol{D}.\nabla C\right) - \frac{n_f \beta_c}{\tilde{C}_{sr}}\frac{\partial C}{\partial t} \tag{2}$$

Salt transport model,

$$\frac{\partial C}{\partial t} = \frac{1}{\bar{\rho}_f}\nabla.\left(\bar{\rho}_f \boldsymbol{D}_h.\nabla C\right) - \left(\frac{\rho_{f0}\beta_c C}{\bar{\rho}_f}\right)\nabla.\left(n_f \boldsymbol{D}.\nabla C\right) - \boldsymbol{v}_f.\nabla C \tag{3}$$

where h_p and y are the pressure and elevation heads of water, $\tilde{C}_{sr} = \left(n_f \rho_f g/K_f\right) + n\left(\rho_f/\rho_{f0}\right)\left(\partial S_r/\partial h_p\right)$, K_f is the bulk modulus of water, k_f is the hydraulic conductivity of soil, $\delta_c = 1 + \beta_c C$, $\beta_c = \rho_s/\rho_{f0} - 1$, μ_r is the relative viscosity, $\bar{\rho}_f = n_f \rho_f$, $n_f = nS_r$ with n and S_r being the soil porosity and degree of saturation of the soil, respectively. $\boldsymbol{D}_h$ is the coefficient of hydrodynamic dispersion, given by,

$$D_h^{mn} = \left[\alpha_t \delta^{mn} + (\alpha_l - \alpha_t)\frac{v_f^m v_f^n}{\left|\boldsymbol{v}_f\right|^2}\right]\left|\boldsymbol{v}_f\right| + D^* T\left(n_f\right)\delta^{mn} \tag{4}$$

In the above equation, $\boldsymbol{v}_f$ is the flow velocity of water, α_l and α_t are the longitudinal and transverse dispersivities, D^* is the coefficient of molecular diffusion, and $T\left(n_f\right) = n_f^{7/3}/n^2$ is the tortuosity factor representing the restriction to flow due to the presence of a pore-structure, while m and n represent the coordinate directions. Lastly, the degree of saturation of the soil in the unsaturated zones is estimated as a function of the pressure (suction) head using the van Genuchten hydraulic constitutive models,

$$S_r = \left[1 + \left(g_a|-h_p|\right)^{g_n}\right]^{g_c} \tag{5}$$

where g_a, g_n, and g_c are model parameters dependent on the soil type.

4. Numerical model

The mathematical model described above is solved as an initial-boundary value problem for various cross-sections of the earth dam using the Smoothed Particle Hydrodynamics (SPH) method. The present section outlines the SPH methodology and numerical modelling of the coupled flow-salt transport process.

4.1 Smoothed Particle Hydrodynamics (SPH) method

The Smoothed Particle Hydrodynamics (SPH) method was originally developed for astrophysics, and later extended to several engineering applications [2,3]. The SPH method is based on the approximation of a field variable f evaluated at coordinate $\boldsymbol{x}$ in the domain Ω,

$$f(\boldsymbol{x}) = \int_{\Omega} f(\boldsymbol{x}')\delta(\boldsymbol{x} - \boldsymbol{x}')dV \tag{6}$$

where dV is the elemental volume at the coordinate $\boldsymbol{x}'$ and $\delta(\boldsymbol{x} - \boldsymbol{x}')$ is the Dirac delta function. The discontinuous Dirac delta function is replaced by a smooth kernel function $W(\boldsymbol{x} - \boldsymbol{x}', h)$, where h is the smoothing length that defines the zone of approximation around $\boldsymbol{x}$. The kernel function is mathematically designed to fulfil the following conditions,

- Compact support, i.e., $W(\boldsymbol{x} - \boldsymbol{x}', h) \to 0$ if $|\boldsymbol{x} - \boldsymbol{x}'| \geq \kappa h$, where κ is a constant.
- Normalization, i.e., $\int_{\Omega} W(\boldsymbol{x} - \boldsymbol{x}', h)dV = 1$.
- Approximating the Dirac delta function as the smoothing length tends to zero, i.e., $W(\boldsymbol{x} - \boldsymbol{x}', h) \approx \delta(\boldsymbol{x} - \boldsymbol{x}')$ as $h \to 0$.

The integral approximation of the Eq. 6 is obtained by replacing the Dirac delta function by the kernel function,

$$f(\boldsymbol{x}) = \int_{\Omega} f(\boldsymbol{x}')W(\boldsymbol{x} - \boldsymbol{x}', h)dV \tag{7}$$

The computational domain is spatially discretized by a finite number of nodes or particles to numerically evaluate the above approximation (Fig. 1). The particles represent a finite volume of the domain and carry field variables, e.g., density, stress, velocity, etc. The SPH approximation for the function f evaluated at a particle i is obtained by summation over neighbour particles,

$$f(\boldsymbol{x}_i) = \sum_j f(\boldsymbol{x}_j)W(\boldsymbol{x}_i - \boldsymbol{x}_j, h)V_j \tag{8}$$

where V_j is the volume of the j^{th} neighbour particle of particle i. The kernel function directly influences the accuracy of the SPH approximation and the overall computational efficiency. The quintic Wendland kernel function is adopted in the present numerical analysis. The quintic Wendland kernel function is given by,

$$W(\boldsymbol{x}_i - \boldsymbol{x}_j, h) = \alpha_d(1 + 2q)(1 - 0.5q)^4 \tag{9}$$

for $q \leq 2$, and 0 otherwise. In the above equation, $q = |\boldsymbol{x}_i - \boldsymbol{x}_j|/h$ is the non-dimensional distance between particles i and j, and $\alpha_d = 7/4\pi h^2$ is the normalization constant for two-dimensional analysis.

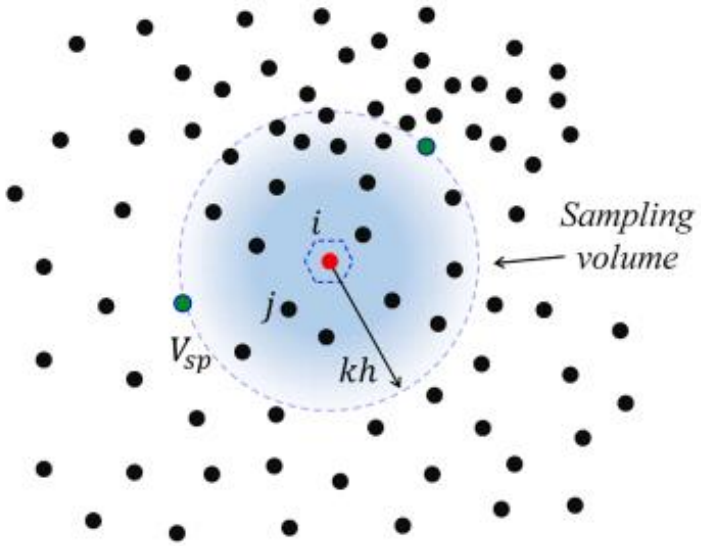

Fig. 1 Domain discretization using the SPH method [3]

The SPH approximation for the first and second-order derivatives of a function f are obtained using Eq. 7 and are given as follows [4],

$$\tilde{\nabla}^m f(\boldsymbol{x}_i) = \sum_j (f_j - f_i)\tilde{\nabla}_i^m W_{ij} V_j \tag{10}$$

$$\frac{\partial^2 f(\boldsymbol{x}_i)}{\partial x^m \partial x^n} = \sum_j (f_j - f_i) E^{mn} \tilde{F}_{ij} V_j - \tilde{\nabla} f(\boldsymbol{x}_i) . \sum_j \boldsymbol{x}_{ji} E^{mn} \tilde{F}_{ij} V_j \tag{11}$$

where $\boldsymbol{x}_i$ is the position vector of particle i, $f_i = f(\boldsymbol{x}_i)$, $\tilde{\nabla}_i W_{ij} = \boldsymbol{L}_{ij} \nabla_i W_{ij}$ is the corrected kernel gradient, $\boldsymbol{L}_{ij} = \left[\sum_j \boldsymbol{x}_{ji}^m \nabla_i^n W_{ij} V_j\right]^{-1}$ is the renormalization matrix, $\nabla_i W_{ij}$ is the uncorrected kernel gradient, $E^{mn} = 4x_{ji}^m x_{ji}^n / |\boldsymbol{x}_{ji}|^2$, $\tilde{F}_{ij} = \boldsymbol{x}_{ji} . \tilde{\nabla}_i W_{ij} / |\boldsymbol{x}_{ji}|^2$, $\boldsymbol{x}_{ji} = \boldsymbol{x}_j - \boldsymbol{x}_i$, while m and n denote the coordinate directions. Eq. 8, 10 and 11 are the fundamental SPH operators and are adopted for spatially discretizing the coupled flow-solute transport model.

4.2 Boundary conditions

The boundary conditions for the flow and solute transport model (Eq. 2 and 3, respectively) are imposed over the SPH particles present at the appropriate location. Additionally, the boundary conditions for the present analysis are dynamic due to the annual variation of the reservoir water level and daily variation of the seawater level (tidal fluctuations). Incorporating the dynamic boundary conditions in the numerical analysis is essential as saltwater influx is expedited during the summer months with low reservoir levels. The boundary conditions used for the numerical analysis are as follows,

- ***Reservoir level:*** The water level in the reservoir demonstrates an annual variation with the water level dropping to the minimum drawdown level (MDDL) during the summer season and reaching the full reservoir level (FRL) during and post monsoon season. The annual variation of the reservoir as provided by NCCR is shown in Fig. 2 and is used for imposing the dynamic boundary condition on the reservoir side.
- ***Seawater level:*** Seawater level is assumed to vary as a sinusoidal function with an amplitude of 6 m about the mean sea level (0 m) and time period of 24 hrs 50 minutes. The corresponding daily variation of the seawater level is shown in Fig. 3.

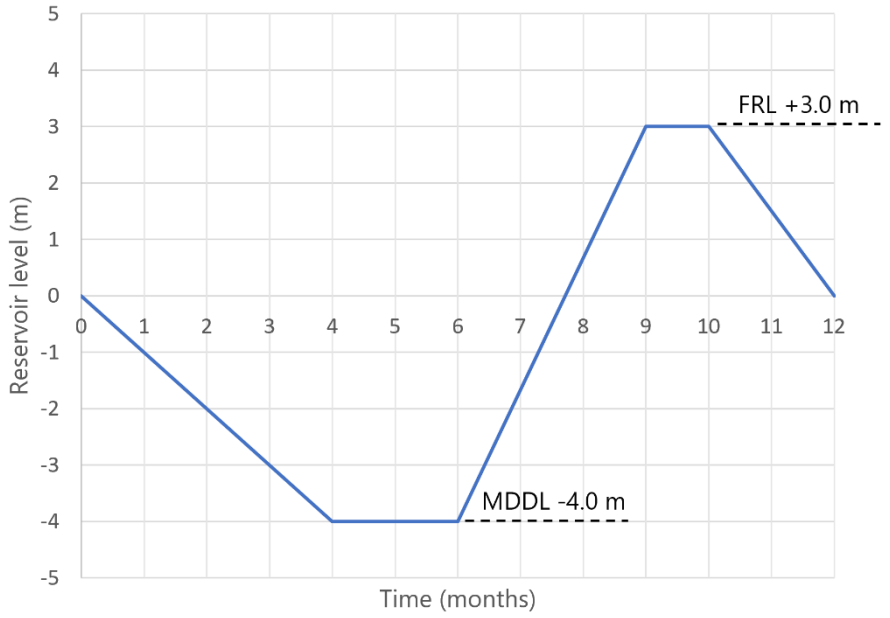

Fig. 2 Annual variation of the reservoir water level (as provided by NCCR)

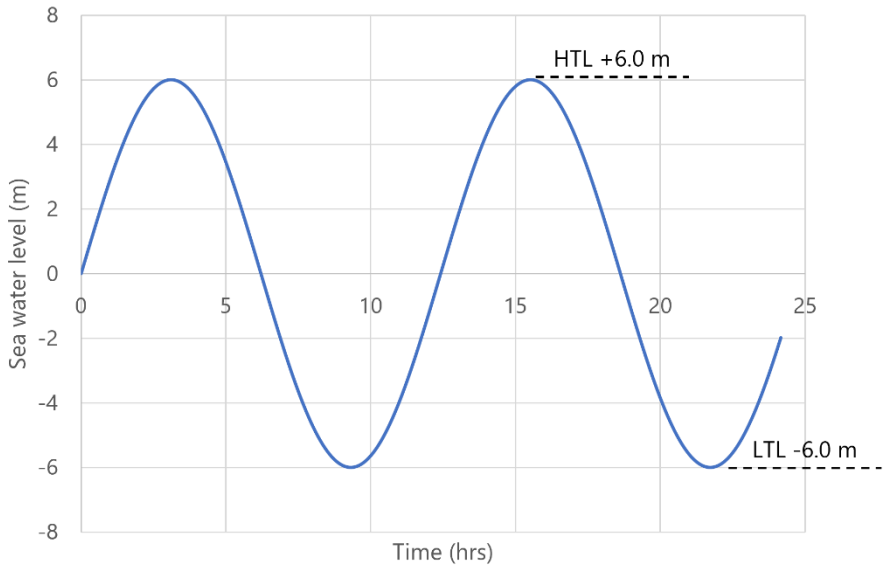

Fig. 3 Daily variation of the seawater level

Lastly, plastic cutoff wall is modelled as an impermeable barrier in the present numerical analysis. In the SPH approach, the impermeable boundary is exactly modelled by neglecting the interaction between particles present on opposite sides of the cutoff wall. It is noteworthy that the impermeable boundary condition used in this analysis assumes that the cutoff wall is constructed with a sufficiently high quality that there are no cracks that may allow flow of water through the wall.

5. Results of the numerical analysis

The present section outlines the numerical modelling of the flow-salt transport process using the SPH method. The mathematical model and boundary conditions are described in Sections 3 and 4. The spatial resolution (particle spacing) used in an SPH simulation governs the numerical accuracy and the computational efficiency. In the present analysis, the domain is discretized using particles placed at a spacing of 1 m on rectangular grid. Additional material parameters utilized for the analysis are summarized in Table 1.

Table 1 Material parameters for the numerical analysis

Parameter	Value
Density	
- Freshwater, ρ_{f0}	1000 kg/m^3
- Seawater, ρ_s	1025 kg/m^3
van Genuchten parameters, (g_a, gn, gl)	(14.5, 2.68, 0.50)
Permeability	
- Seabed (sand)	6.5×10^{-5} m/s
- Dredged material	5.0×10^{-5} m/s
- Clay	4.3×10^{-7} m/s
Viscosity	
- Freshwater	1.0×10^{-3} Pa.s
- Seawater	1.09×10^{-3} Pa.s
Dispersivity, α_l and α_t	20 m and 2 m for 0 m, +2 m, & +5 m sections.
	30 m and 3 m for all other sections.
Coefficient of molecular diffusion, D^*	1.0×10^{-9} m^{2}s^{-1}

The van Genuchten parameters correspond to typical values for sand as per the USDA series [5]. Further, laboratory and field studies available in the literature indicate that the longitudinal dispersivity increases with the overall flow length (directly proportional to the domain dimensions). This is due to the flow of water and dissolved salt through zones of varying permeability (i.e., influence of soil heterogeneity). Typical value of longitudinal dispersivity $\alpha_l \approx 1/10^{\text{th}}$ of the domain dimension (Fig. 4) [1,6,7]. Similarly, the transverse dispersivity $\alpha_t \approx 1/10^{\text{th}}$ of α_l. For the current earth dam geometry, typical flow length (domain dimension) is conservatively assumed to be 200 m for 0 m, +2 m and +5 m sections and 300 m for all other sections. Lastly, the influence of the molecular diffusion on the overall salt transport at the field scale is negligible. This is evident from the small value of the coefficient of molecular diffusion (D^*). Nevertheless, molecular diffusion is included in the numerical analysis.

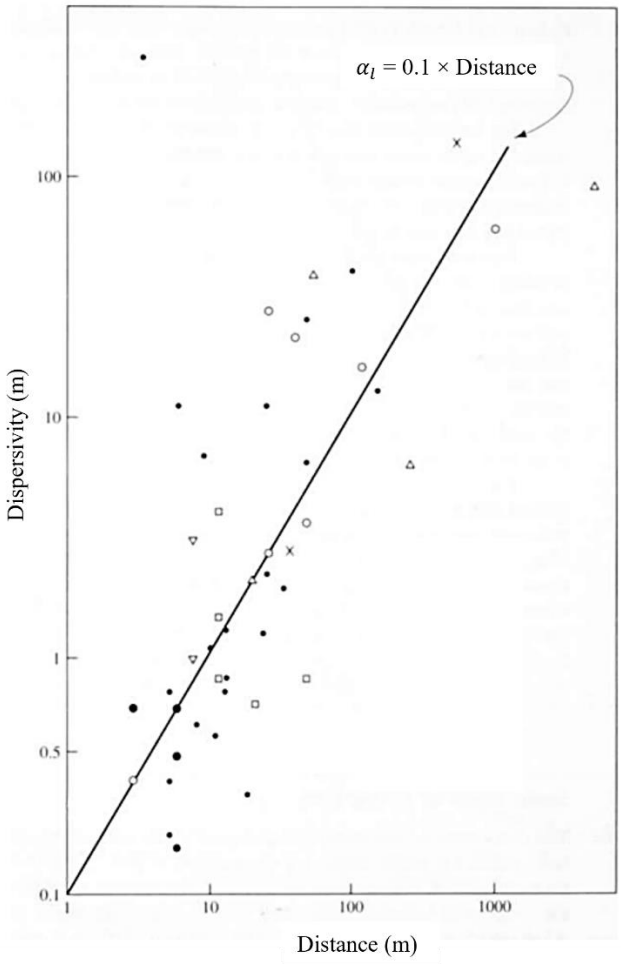

Fig. 4 Longitudinal dispersivities relation with flow distance (after Fetter et al.[6])

5.1 Parametric study on the -15 m section

The section at -15 m depth (Fig. 5) is most frequently encountered along the length of the embankment. As a result, it is adopted for a parametric study on the influence of longitudinal and transverse dispersivities on the coupled flow-salt transport process. The magnitude of dispersivity represents the heterogeneous nature of the porous medium with permeable soil layers (e.g., sand) resulting in an increased salt transport rate.

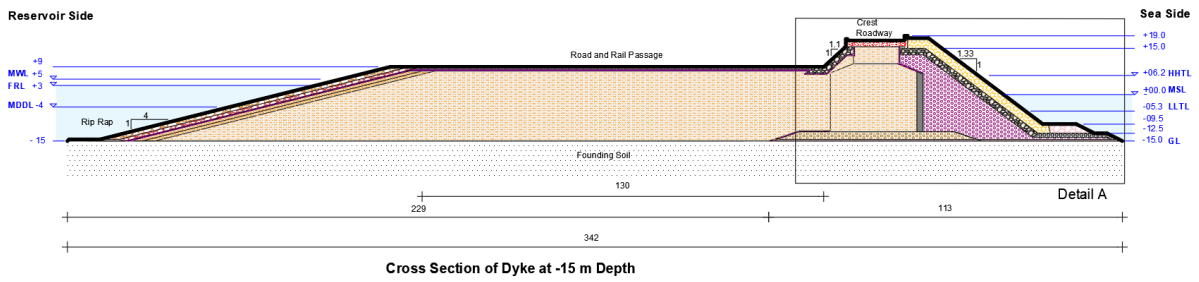

Fig. 5 Cross-section of embankment at -15 m depth

The depth of seabed is also varied in the numerical analysis. A depth of 80 to 100 m of seabed is selected as the flow velocity vectors become horizontal beyond this depth. The results of the numerical analysis for longitudinal dispersivity values of 30 m, 10 m, and 5 m is shown in Fig. 6 to 8. As shown in Figs. 6 to 8, a higher dispersivity value results in higher salt transport, with the 5% isohaline reaching the freshwater reservoir in 210, 510, and 650 days, respectively. To provide a conservative estimate of the transport salt quantities, dispersivity value of 30 m is adopted in the numerical analysis of the remaining cross-sections.

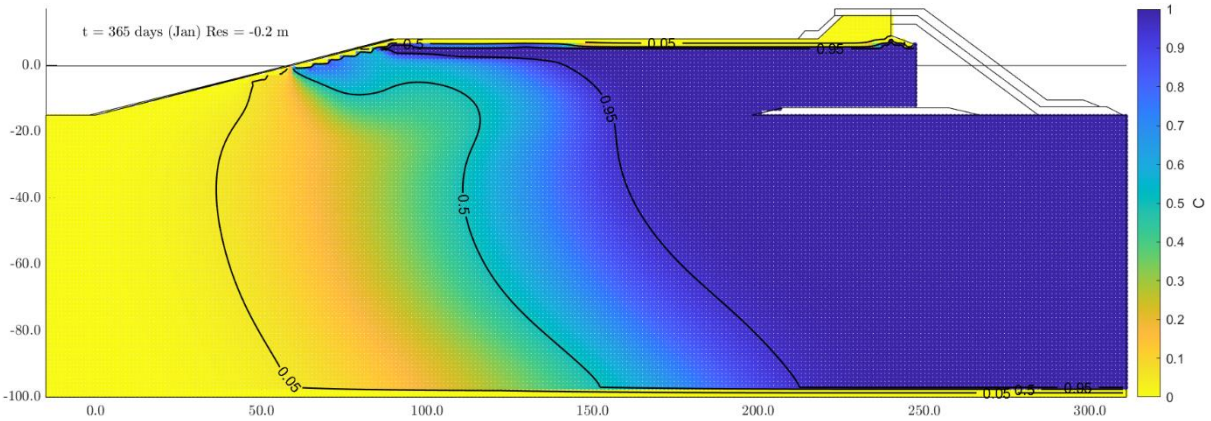

Fig. 6 Normalized salt mass fraction at 1 year with α_l = 30 m, α_t = 3 m

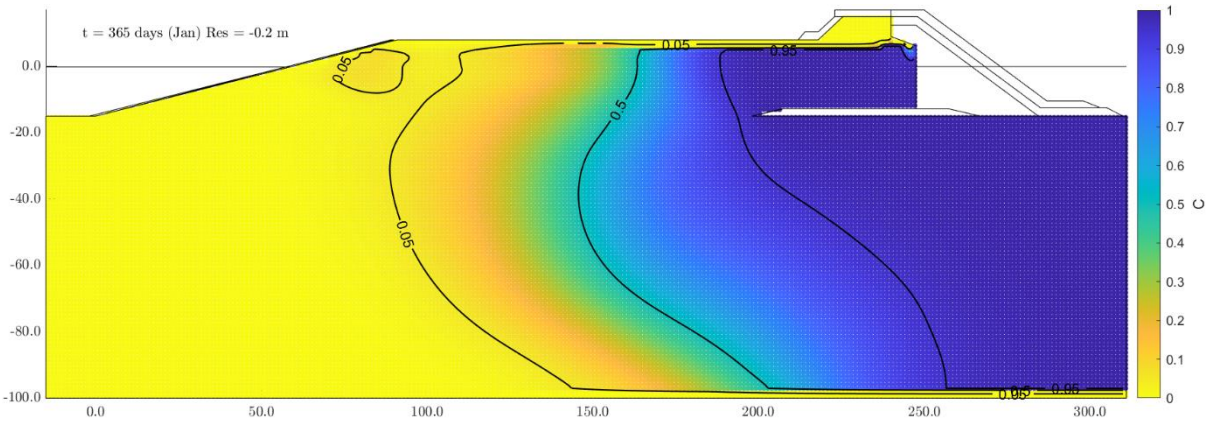

Fig. 7 Normalized salt mass fraction at 1 year with α_l = 10 m, α_t = 1 m

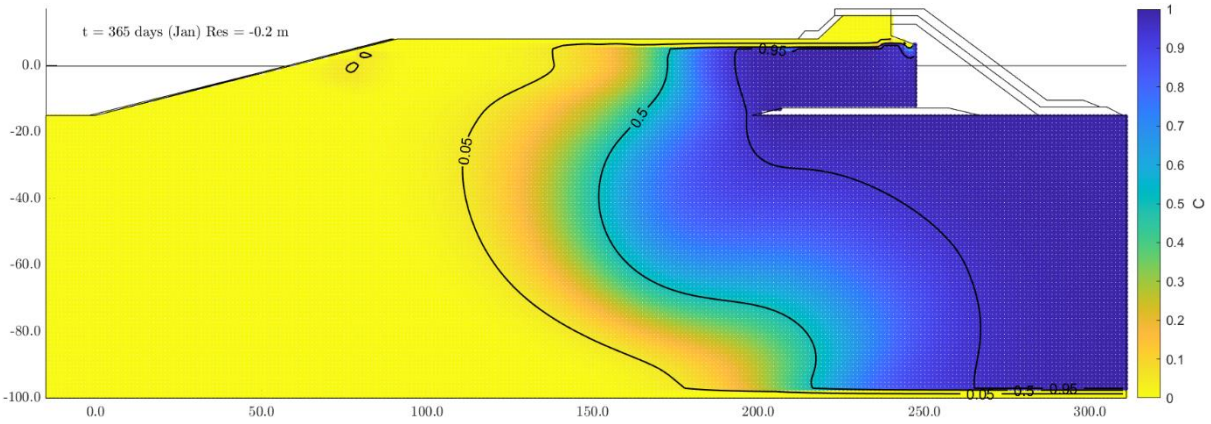

Fig. 8 Normalized salt mass fraction at 1 year with α_l = 5 m, α_t = 0.5 m

Additionally, feasibility of plastic cutoff wall in delaying the saltwater intrusion is also examined. As shown in Fig. 9 to 11, an 80 m deep plastic cutoff wall is modelled as an impermeable boundary. Compared to the case without cutoff wall, the saltwater intrusion in the freshwater reservoir is delayed for all values of dispersivities. As a result, plastic cutoff wall may be adopted for reducing the amount of saltwater intrusion in the reservoir.

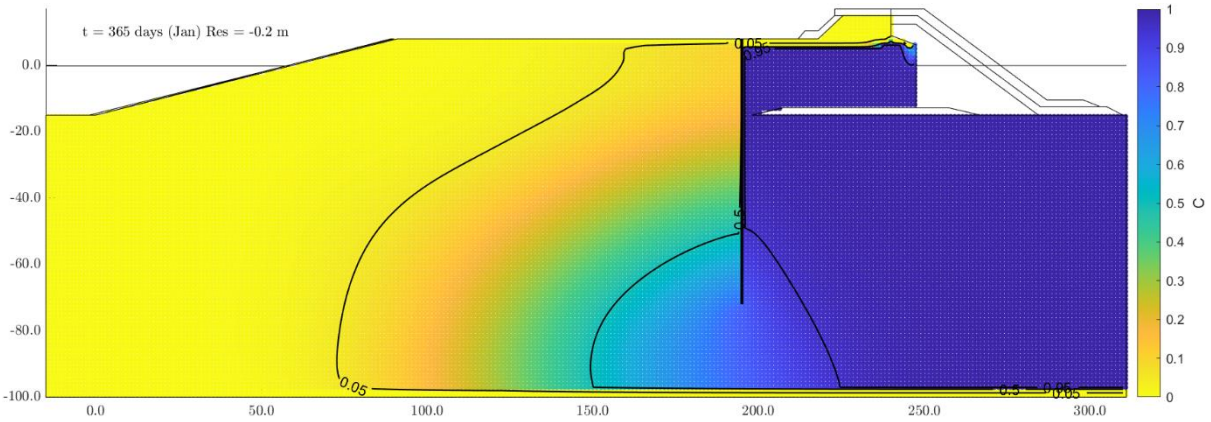

Fig. 9 Normalized salt mass fraction at 1 year with α_l = 30 m, α_t = 3 m, and 80 m deep plastic cutoff wall

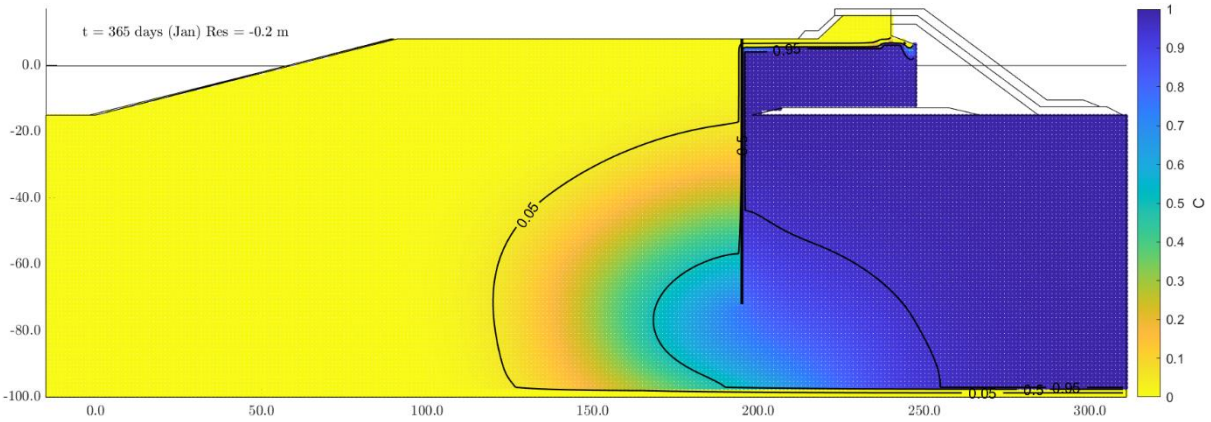

Fig. 10 Normalized salt mass fraction at 1 year with α_l = 10 m, α_t = 1 m, and 80 m deep plastic cutoff wall

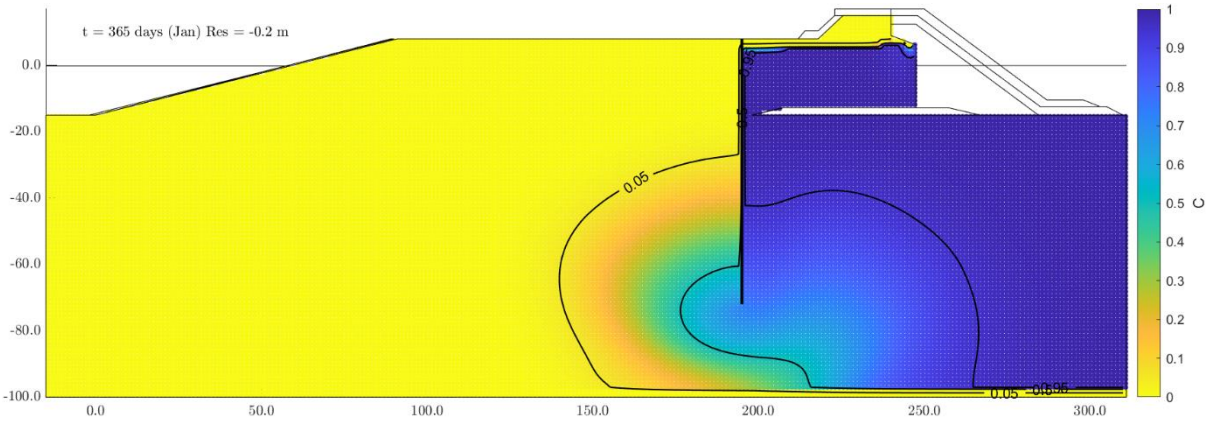

Fig. 11 Normalized salt mass fraction at 1 year with α_l = 5 m, α_t = 0.5 m, and 80 m deep plastic cutoff wall

To quantify the saltwater intrusion, the total volume of water and salt mass transported across various vertical sections of the -15 m cross-sections are estimated. The various vertical sections are shown in Fig. 12.

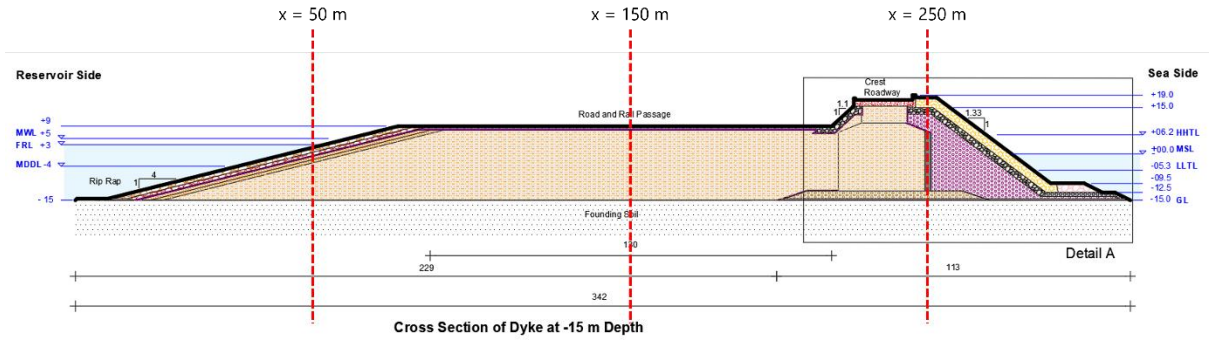

Fig. 12 Cross-sections along the -15 m embankment section

Figs. 13 to 18 illustrate the annual variation of the flow quantity across various sections of the -15 m cross-section. Additionally, the total quantity of water flowing through the embankment and foundation in 1 year is shown in Tables 2 and 3.

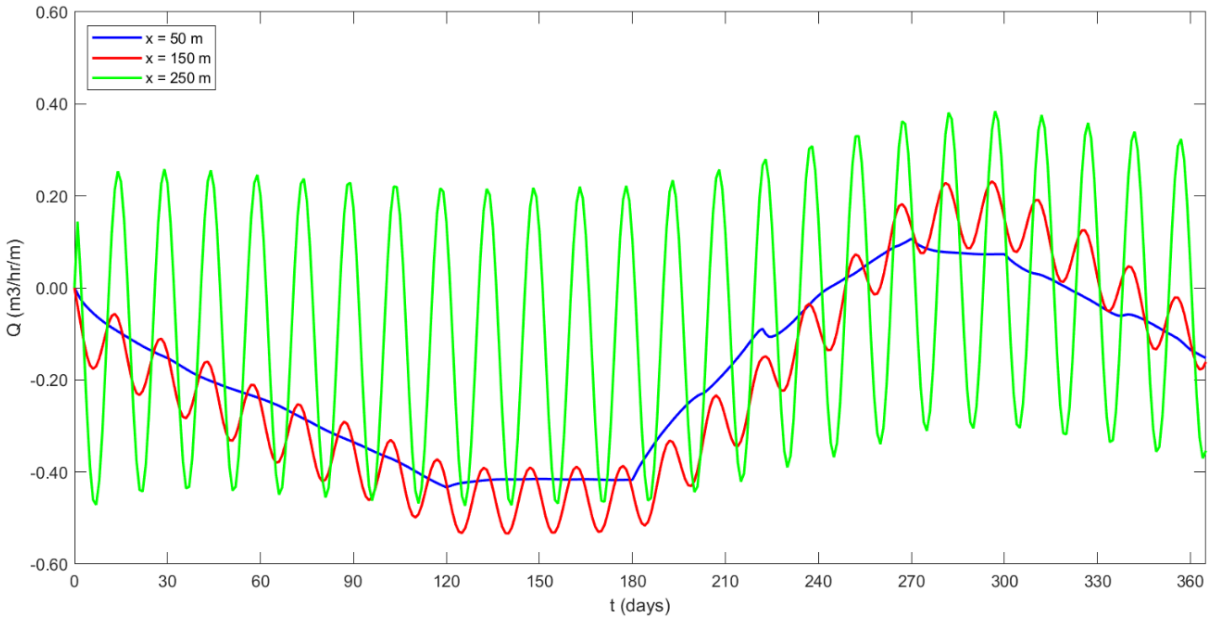

Fig. 13 Annual variation of flow quantity across various cross-sections of -15 m section with α_l = 30 m, α_t = 3 m

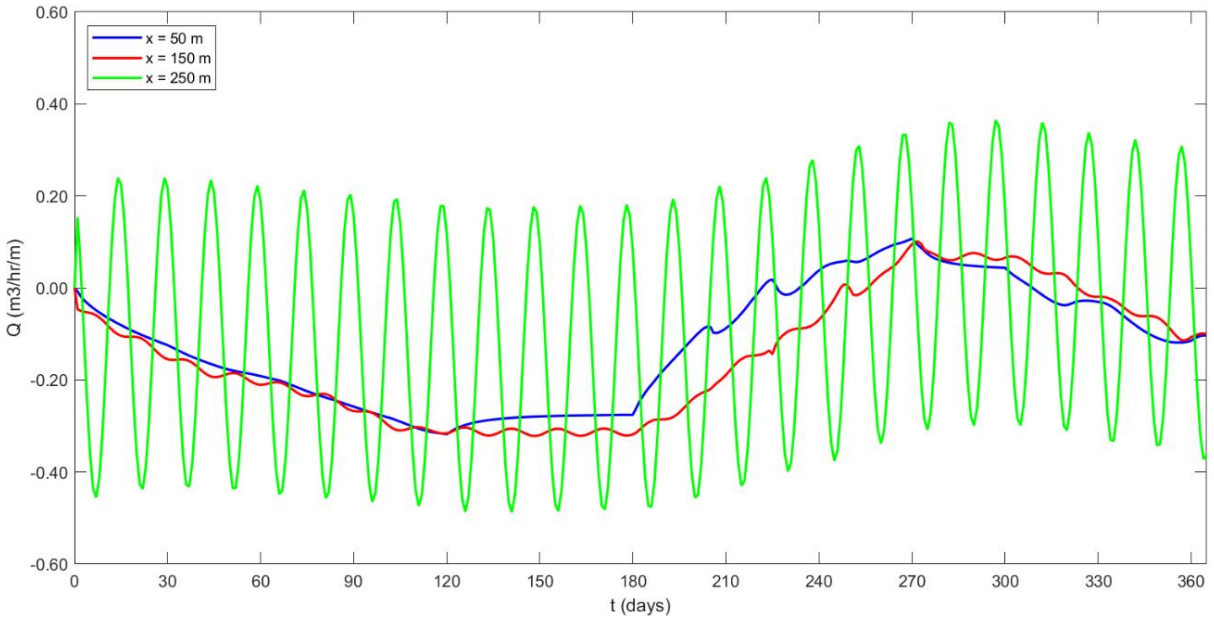

Fig. 14 Annual variation of flow quantity across various cross-sections of -15 m section with α_l = 30 m, α_t = 3 m, and 80 m deep plastic cutoff wall

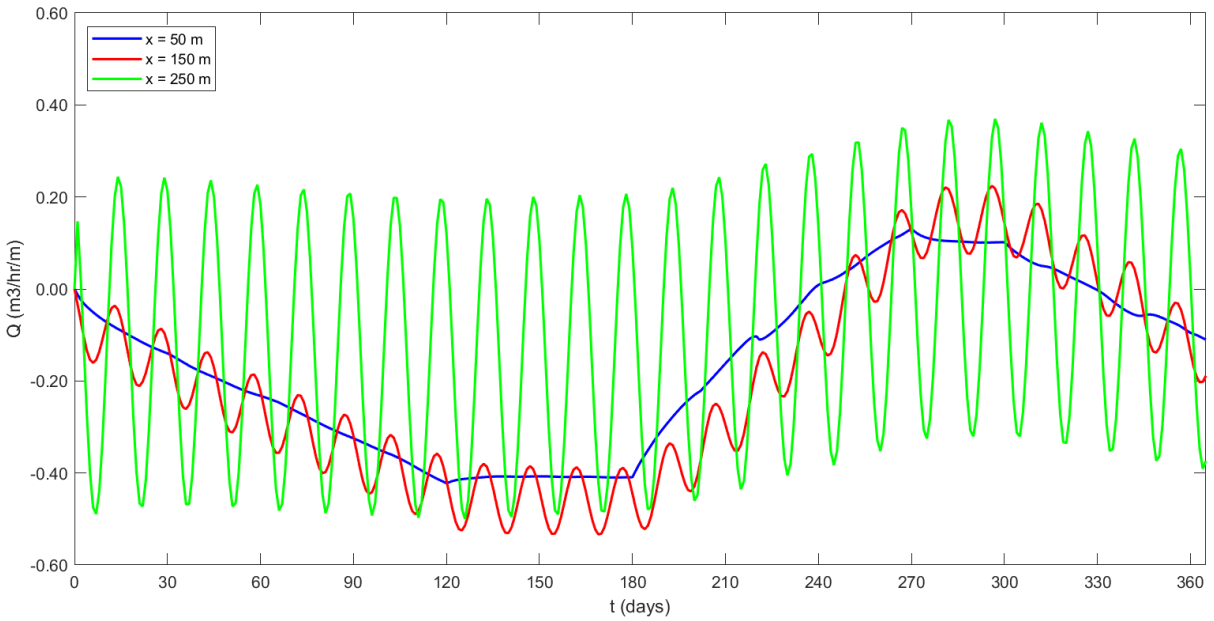

Fig. 15 Annual variation of flow quantity across various cross-sections of -15 m section with α_l = 10 m, α_t = 1 m

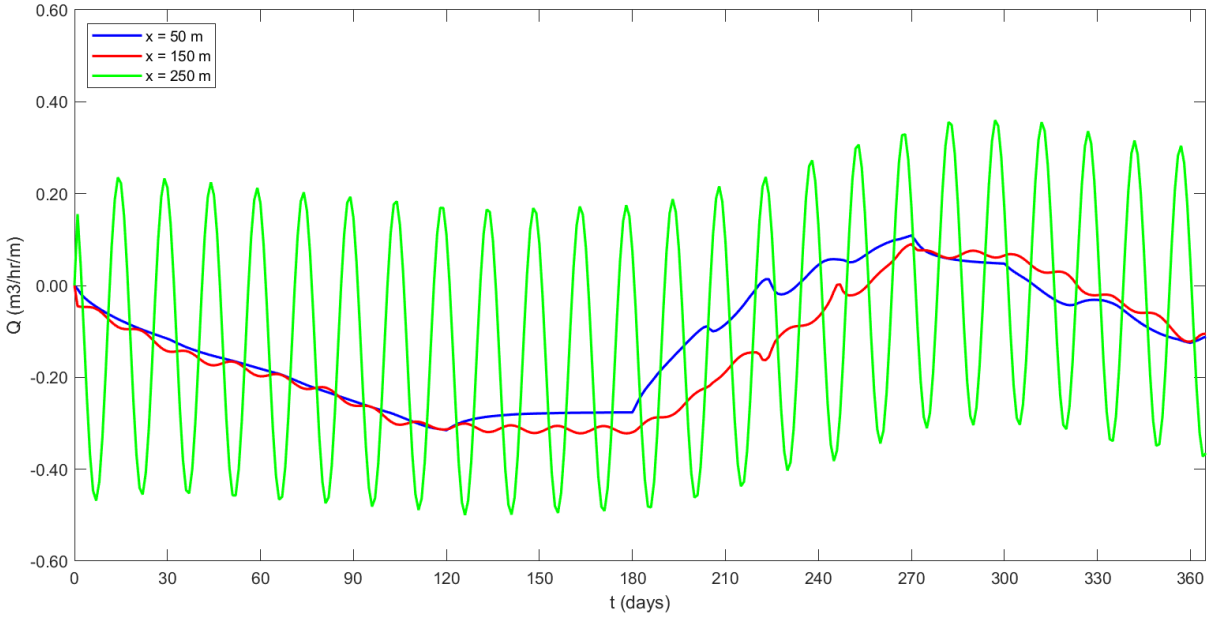

Fig. 16 Annual variation of flow quantity across various cross-sections of -15 m section with α_l = 10 m, α_t = 1 m, and 80 m deep plastic cutoff wall

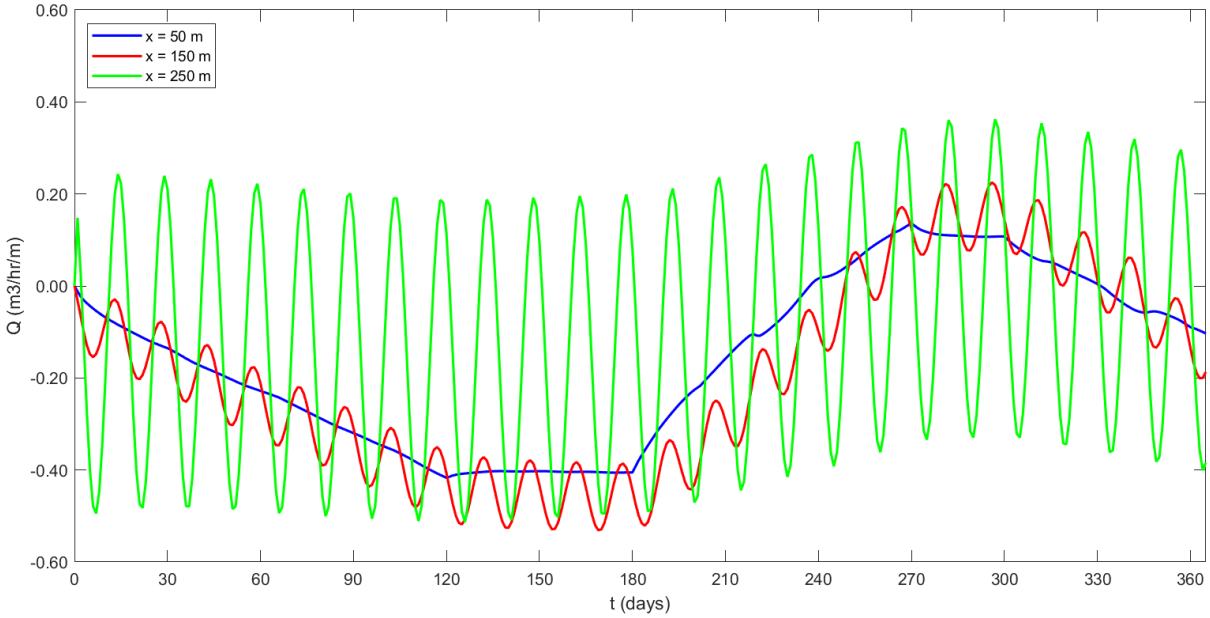

Fig. 17 Annual variation of flow quantity across various cross-sections of -15 m section with α_l = 5 m, α_t = 0.5 m

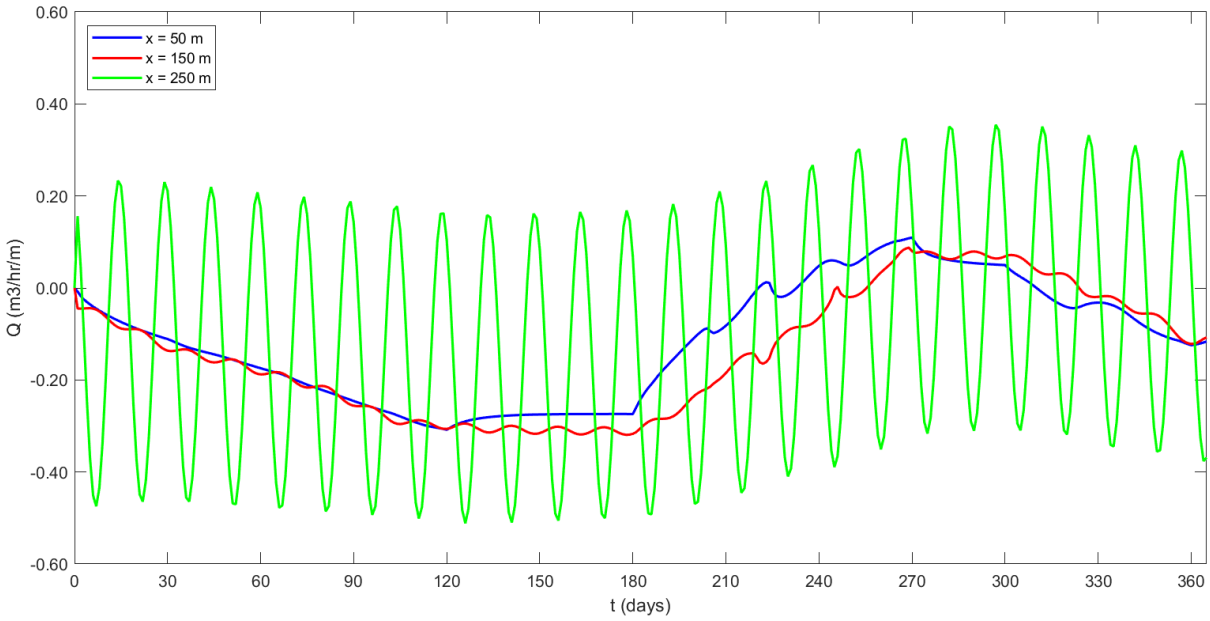

Fig. 18 Annual variation of flow quantity across various cross-sections of -15 m section with α_l = 5 m, α_t = 0.5 m, and 80 m deep plastic cutoff wall

Table 2 Total quantity of water (m^3/m) flowing through the embankment in 1 year at -15 m section

	50 m	**150 m**	**250 m**
α_l = 30 m	-260	-37	0
α_l = 30 m with cutoff	-194	-55	0
α_l = 10 m	-267	-27	0
α_l = 10 m with cutoff	-195	-67	0
α_l = 5 m	-267	-25	0
α_l = 5 m with cutoff	-192	-74	0

Table 3 Total quantity of water (m^3/m) flowing through the embankment in 1 year at -15 m section

	50 m	**150 m**	**250 m**
α_l = 30 m	-1542	-1729	-592
α_l = 30 m with cutoff	-1063	-1282	-719
α_l = 10 m	-1405	-1705	-755
α_l = 10 m with cutoff	-1035	-1256	-790
α_l = 5 m	-1363	-1669	-830
α_l = 5 m with cutoff	-1007	-1217	-850

Figs. 19 to 24 illustrate the annual variation of the salt mass flux (gm/m/s) across various sections of the -15 m cross-section. Additionally, the cumulative salt mass flux through the embankment and foundation in 1 year is shown in Tables 4 and 5.

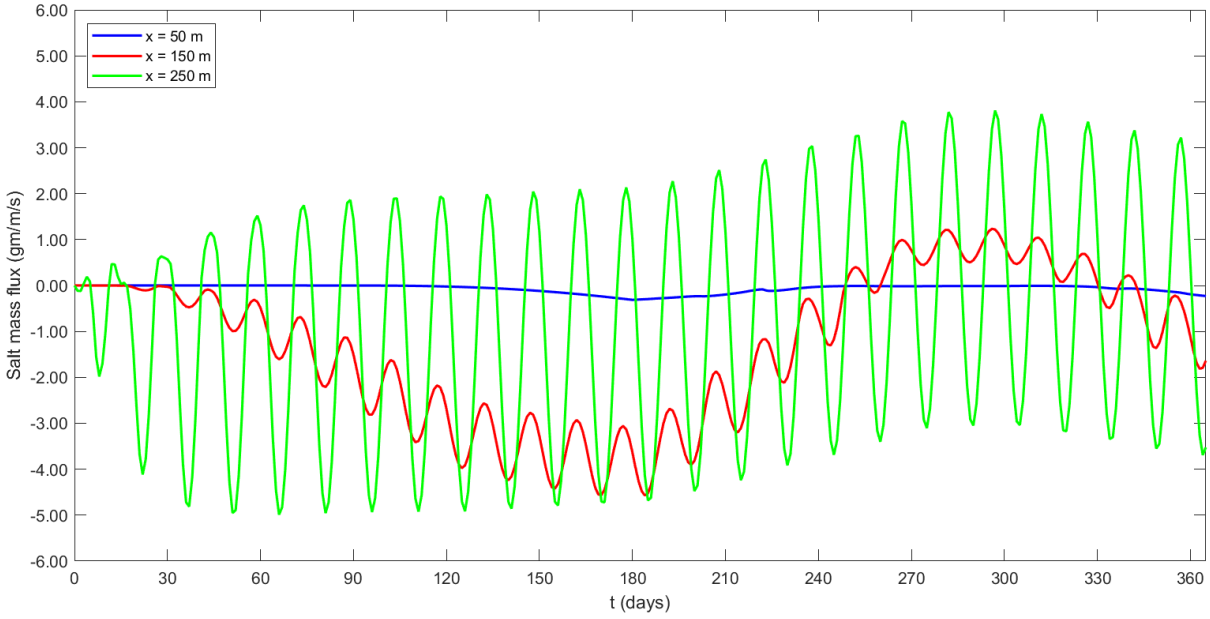

Fig. 19 Annual variation of salt mass flux across various cross-sections of -15 m section with α_l = 30 m, α_t = 3 m

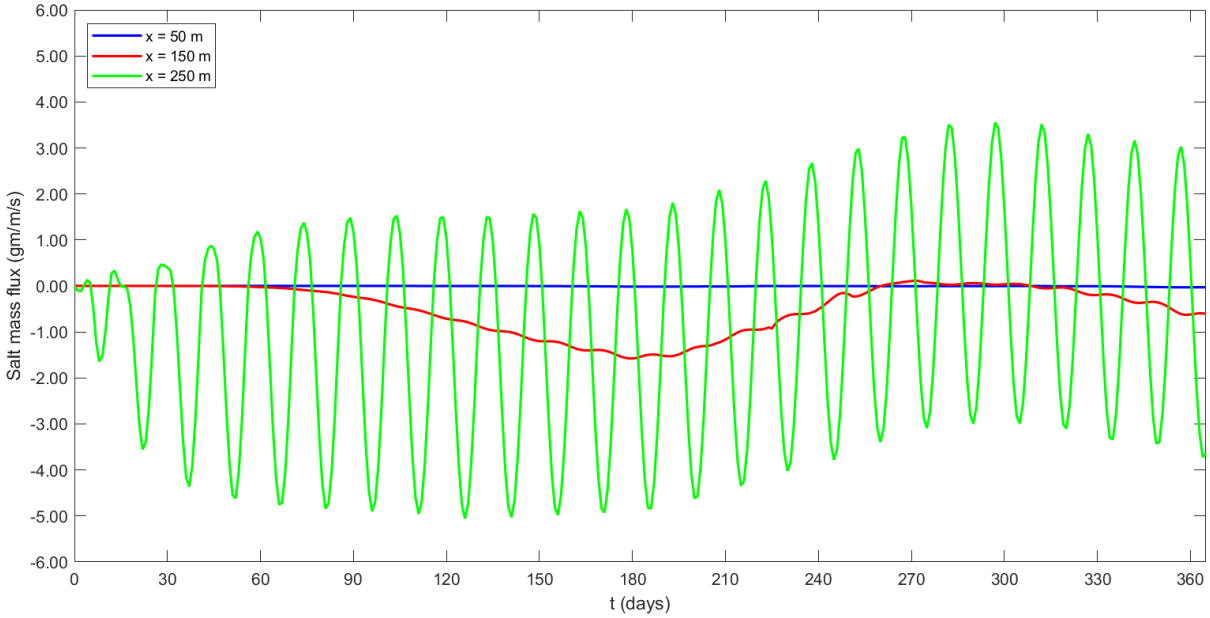

Fig. 20 Annual variation of salt mass flux across various cross-sections of -15 m section with α_l = 30 m, α_t = 3 m, and 80 m deep plastic cutoff wall

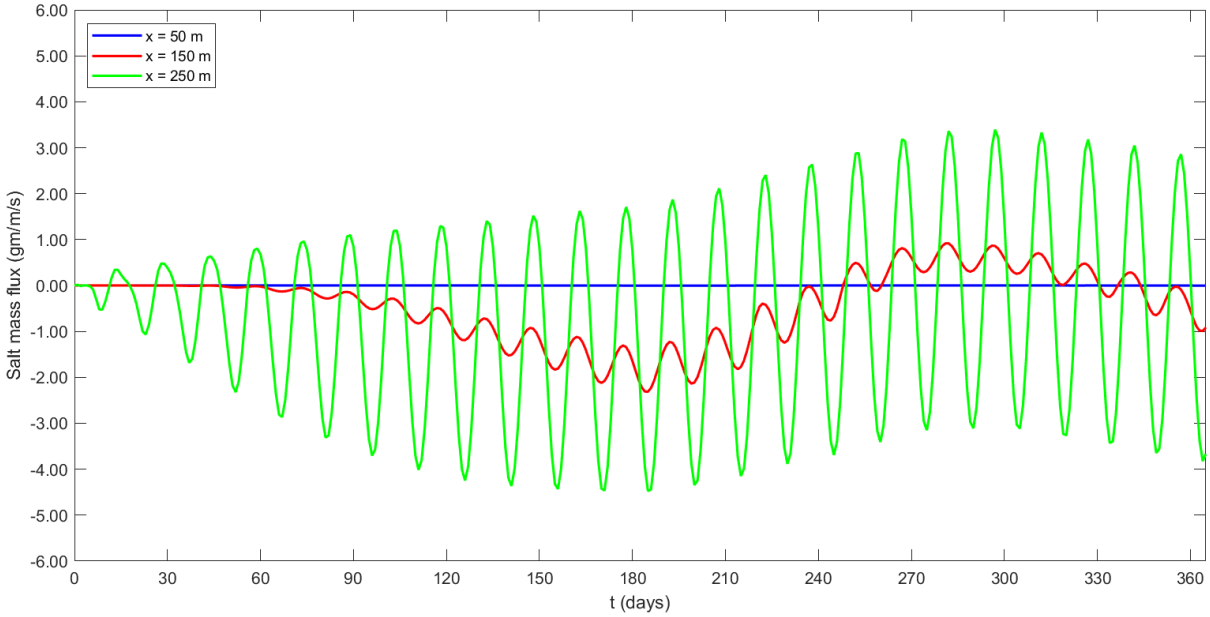

Fig. 21 Annual variation of salt mass flux across various cross-sections of -15 m section with α_l = 10 m, α_t = 1 m

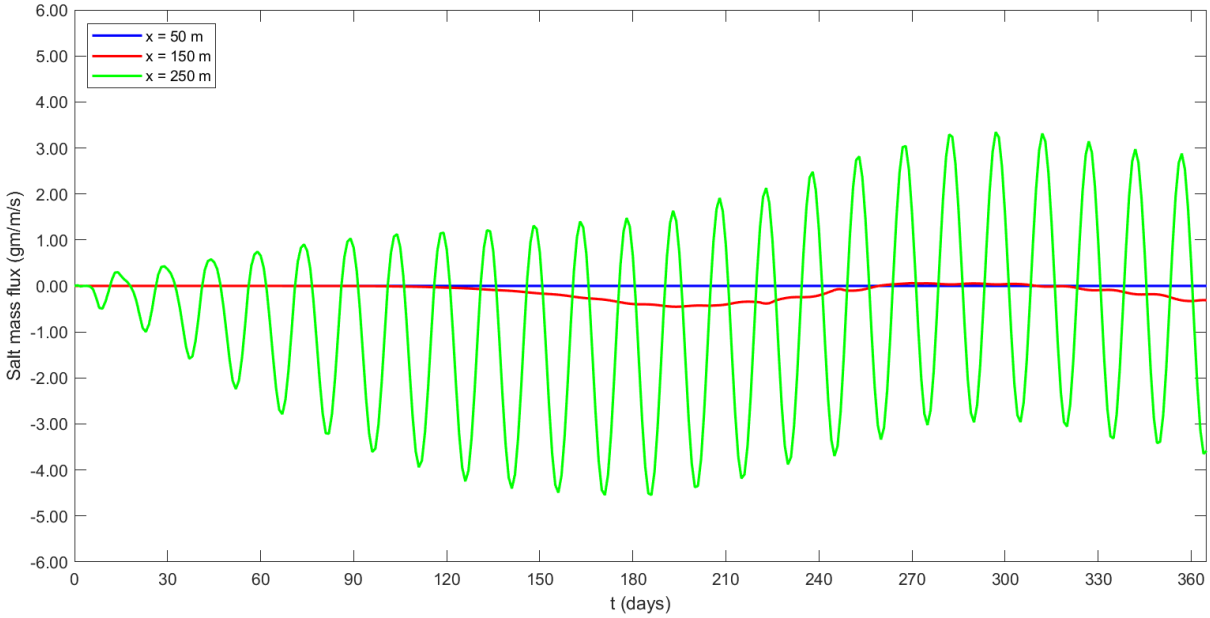

Fig. 22 Annual variation of salt mass flux across various cross-sections of -15 m section with α_l = 10 m, α_t = 1 m, and 80 m deep plastic cutoff wall

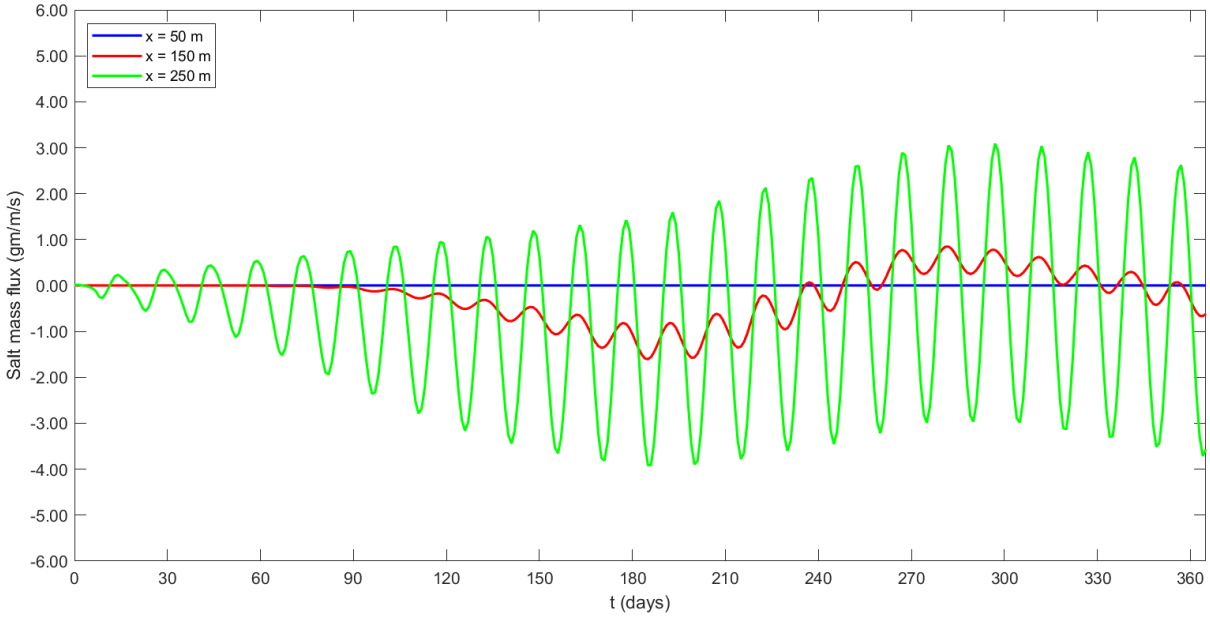

Fig. 23 Annual variation of salt mass flux across various cross-sections of -15 m section with α_l = 5 m, α_t = 0.5 m

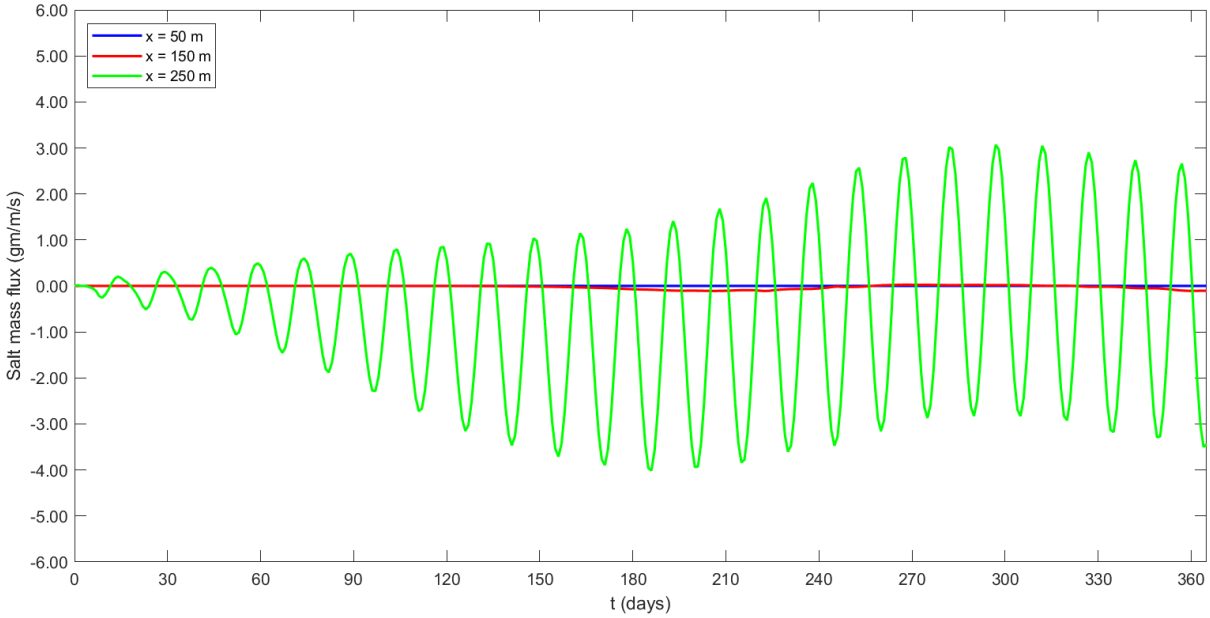

Fig. 24 Annual variation of salt mass flux across various cross-sections of -15 m section with α_l = 5 m, α_t = 0.5 m, and 80 m deep plastic cutoff wall

Table 4 Total quantity of salt mass (kg/m) transported through embankment in 1 year at -15 m section

	50 m	**150 m**	**250 m**
α_l = 30 m	-329	-2830	0
α_l = 30 m with cutoff	-2.5	-0.9	0
α_l = 10 m	-5.6	-554	0
α_l = 10 m with cutoff	0	1.3	0
α_l = 5 m	0	69	0
α_l = 5 m with cutoff	0	0	0

Table 5 Total quantity of salt mass (kg/m) transported through foundation in 1 year at -15 m section

	50 m	**150 m**	**250 m**
α_l = 30 m	-2100	-40500	-23700
α_l = 30 m with cutoff	-156	-14800	-28300
α_l = 10 m	-17	-13175	-20600
α_l = 10 m with cutoff	0	-3500	-21700
α_l = 5 m	-0.1	-6600	-16600
α_l = 5 m with cutoff	0	-710	-17100

5.2 Analysis of other cross-sections

The results of the numerical analysis of other cross-sections of the embankment (i.e., -5 m, -30 m, -25 m, -20 m, -10 m, 0 m, +2 m, and +5 m) and the flood regulator are summarized in this subsection.

5.2.1 -5 m section

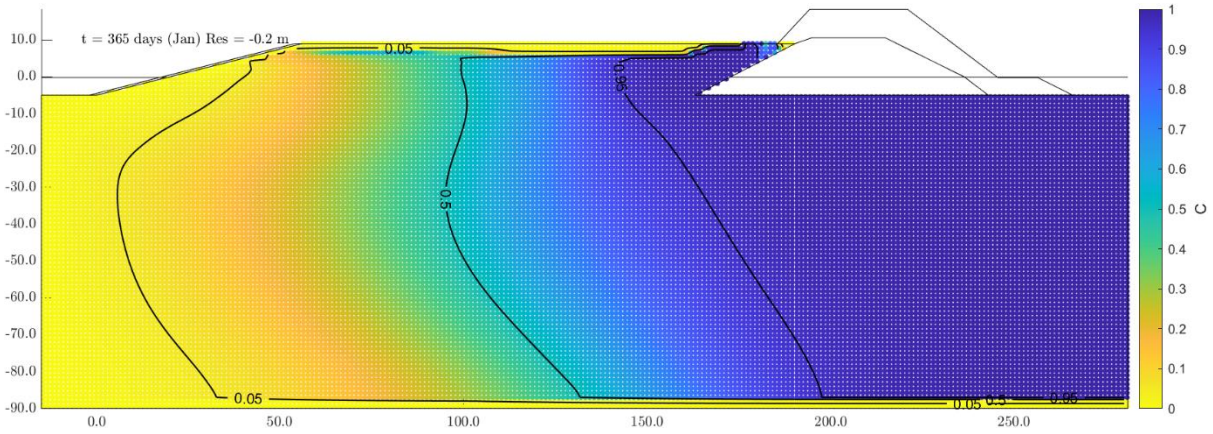

Fig. 25 Normalized salt mass fraction at 1 year for -5 m section with α_l = 30 m, α_t = 3 m

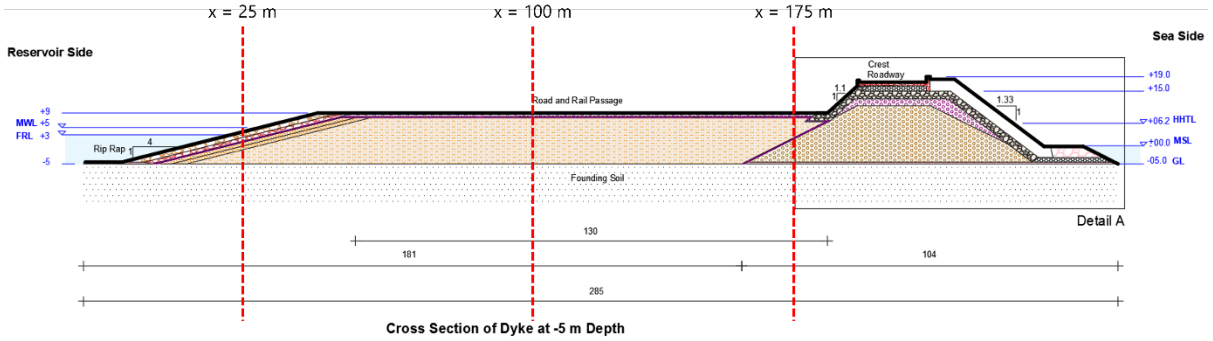

Fig. 26 Cross-sections along the -5 m embankment section

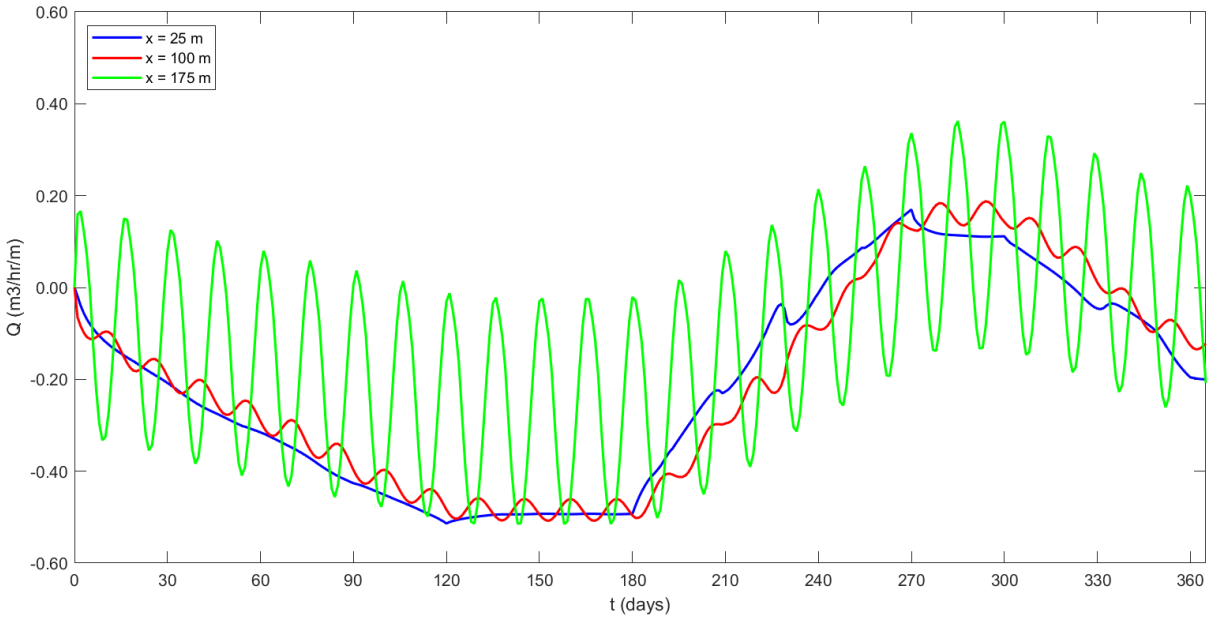

Fig. 27 Annual variation of flow quantity across various cross-sections of -5 m section with α_l = 30 m, α_t = 3 m

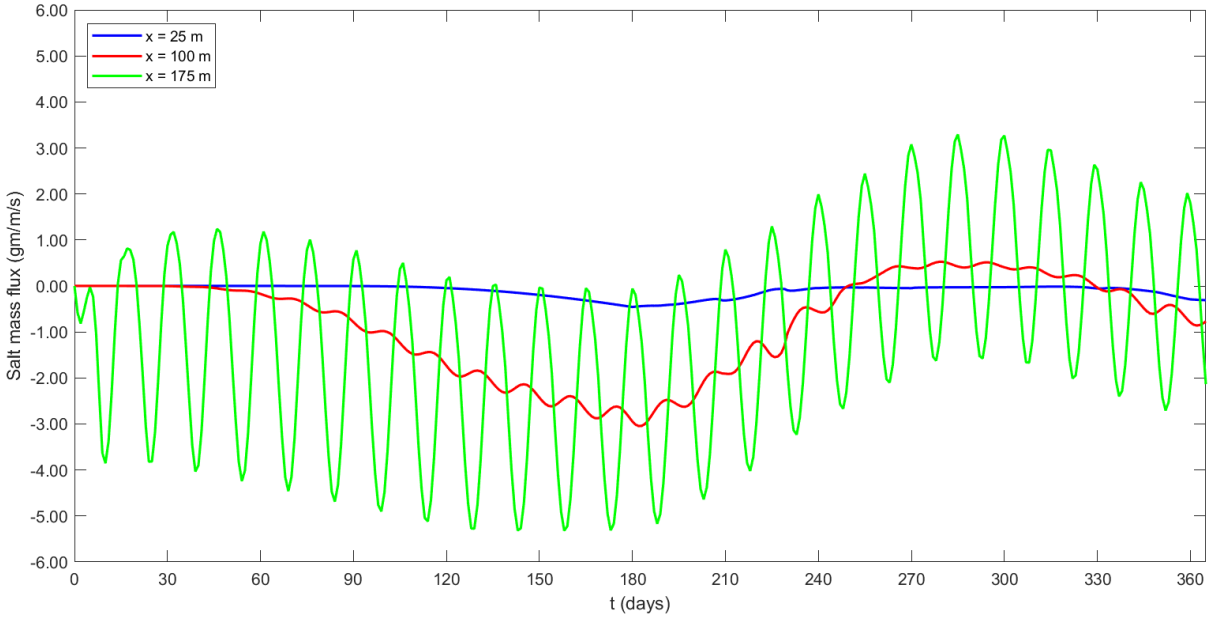

Fig. 28 Annual variation of salt mass flux across various cross-sections of -5 m section with α_l = 30 m, α_t = 3 m

5.2.2 -30 m section

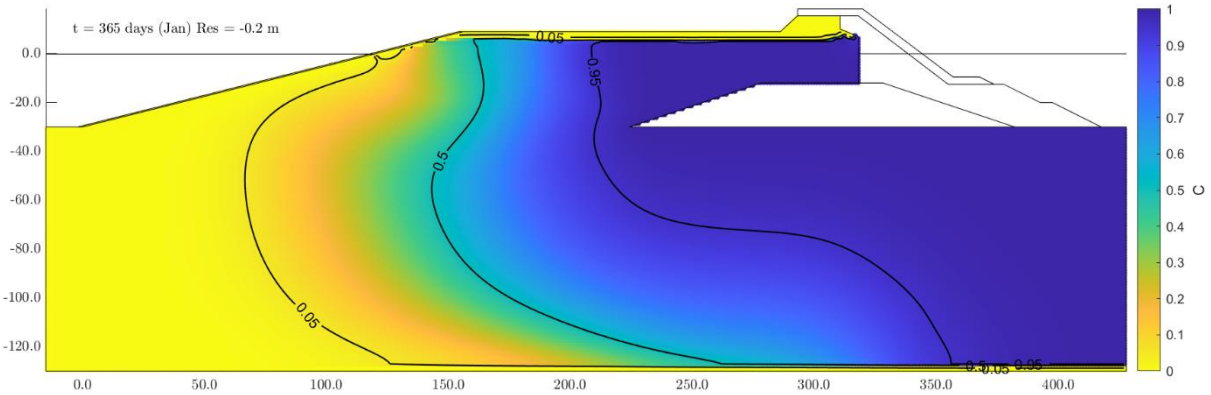

Fig. 29 Normalized salt mass fraction at 1 year for -30 m section with α_l = 30 m, α_t = 3 m

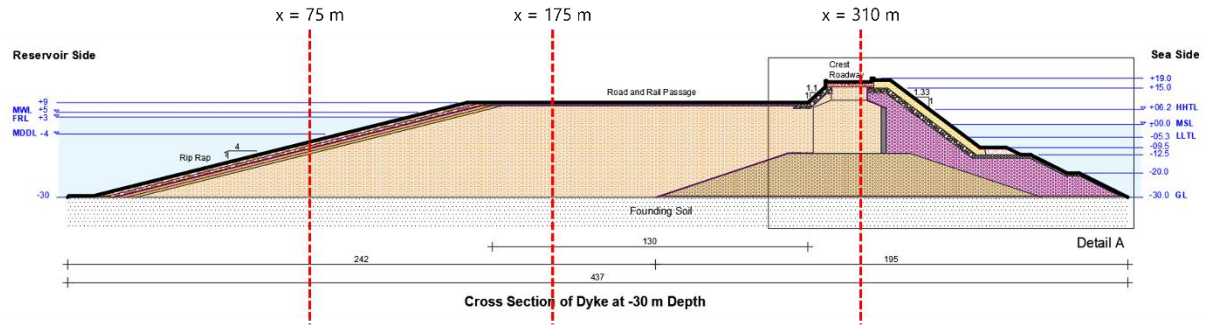

Fig. 30 Cross-sections along the -30 m embankment section

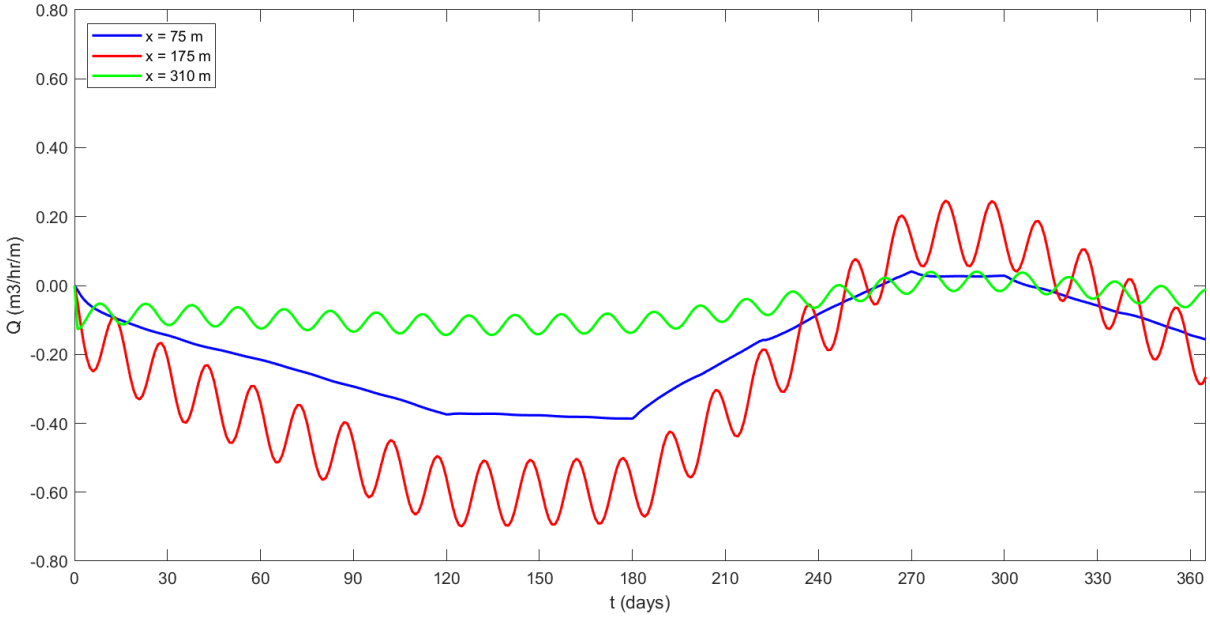

Fig. 31 Annual variation of flow quantity across various cross-sections of -30 m section with α_l = 30 m, α_t = 3 m

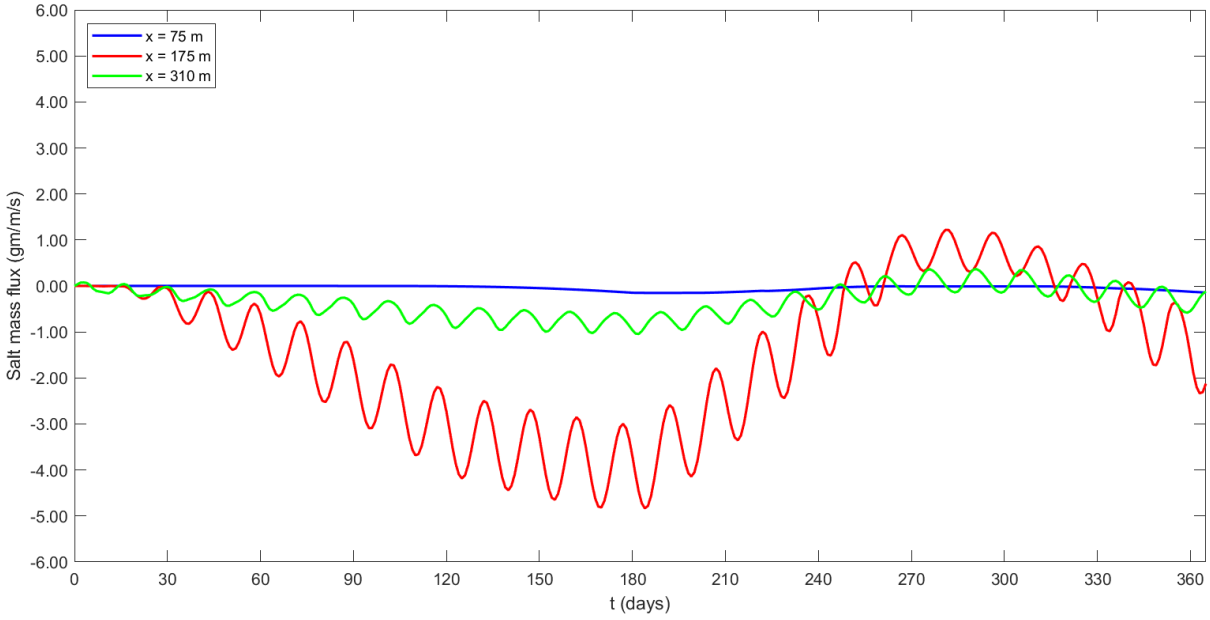

Fig. 32 Annual variation of salt mass flux across various cross-sections of -30 m section with α_l = 30 m, α_t = 3 m

5.2.3 -25 m section

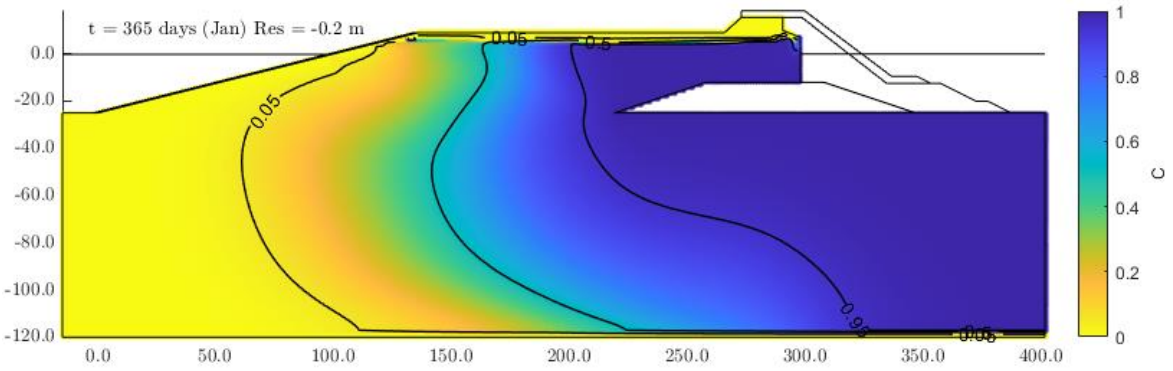

Fig. 33 Normalized salt mass fraction at 1 year for -25 m section with α_l = 30 m, α_t = 3 m

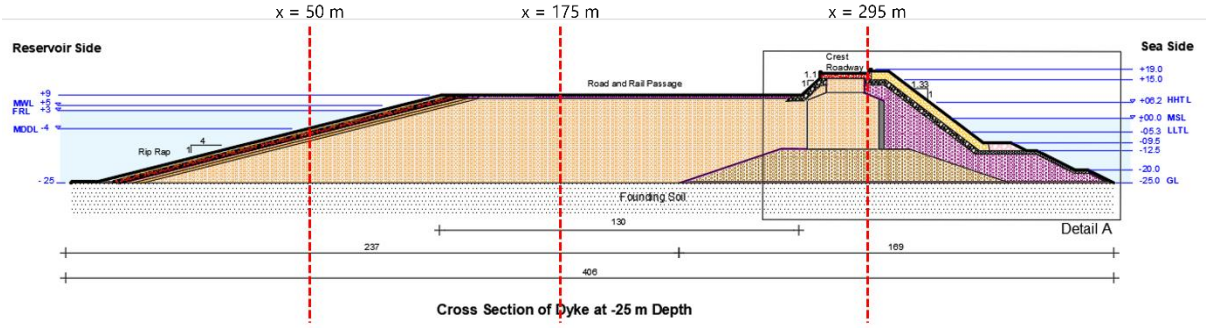

Fig. 34 Cross-sections along the -25 m embankment section

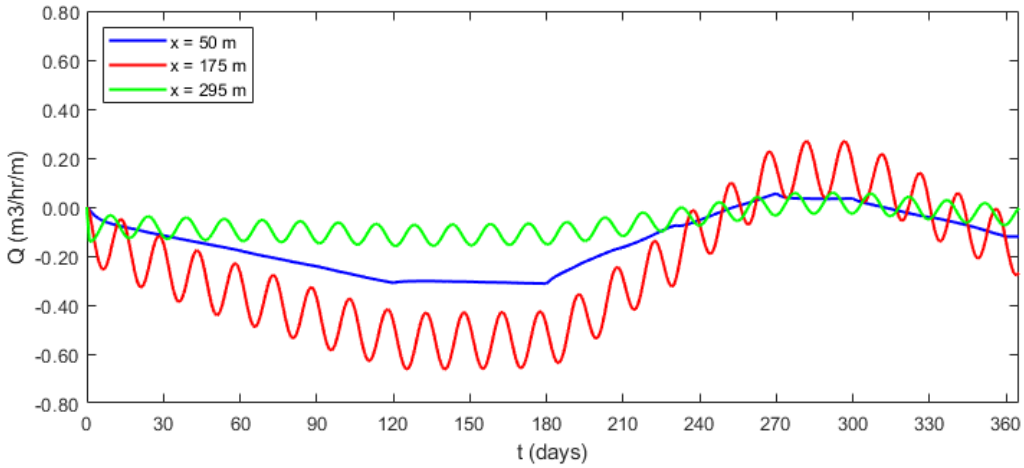

Fig. 35 Annual variation of flow quantity across various cross-sections of -25 m section with α_l = 30 m, α_t = 3 m

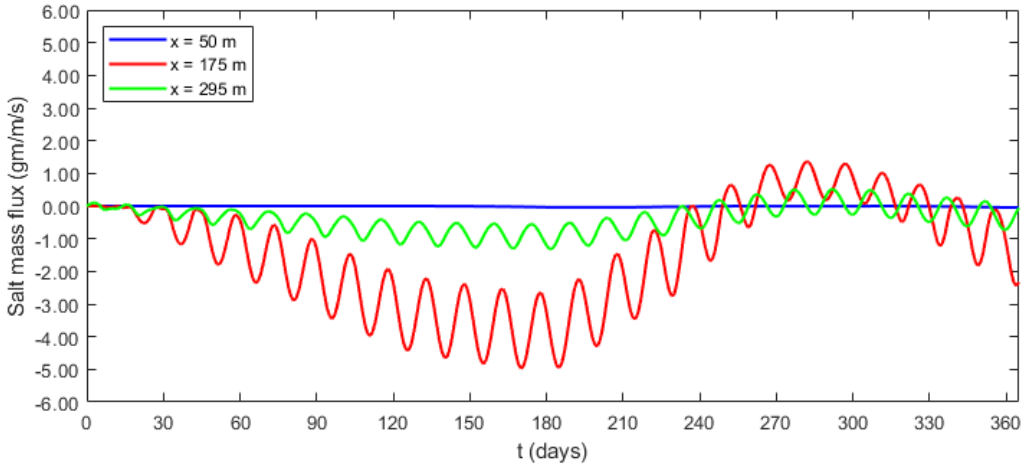

Fig. 36 Annual variation of salt mass flux across various cross-sections of -25 m section with α_l = 30 m, α_t = 3 m

5.2.4 -20 m section

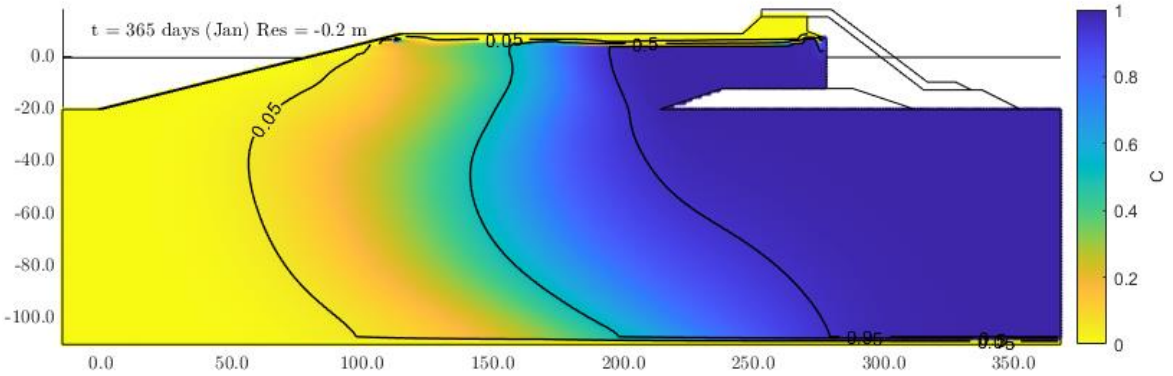

Fig. 37 Normalized salt mass fraction at 1 year for -20 m section with α_l = 30 m, α_t = 3 m

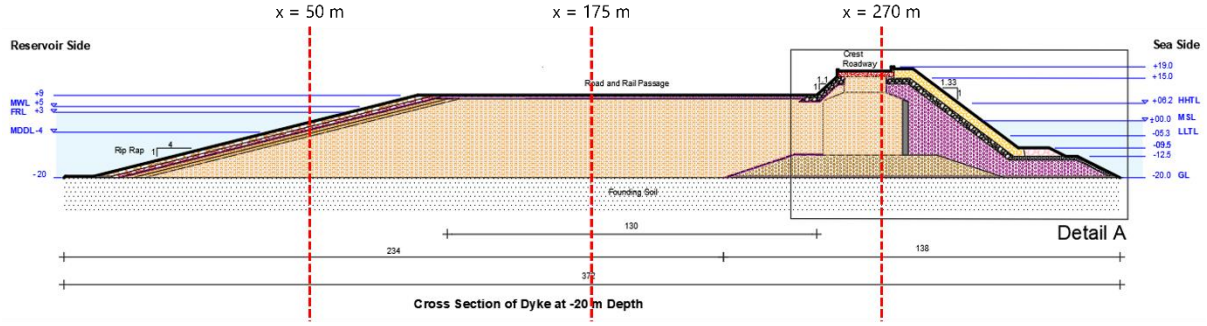

Fig. 38 Cross-sections along the -20 m embankment section

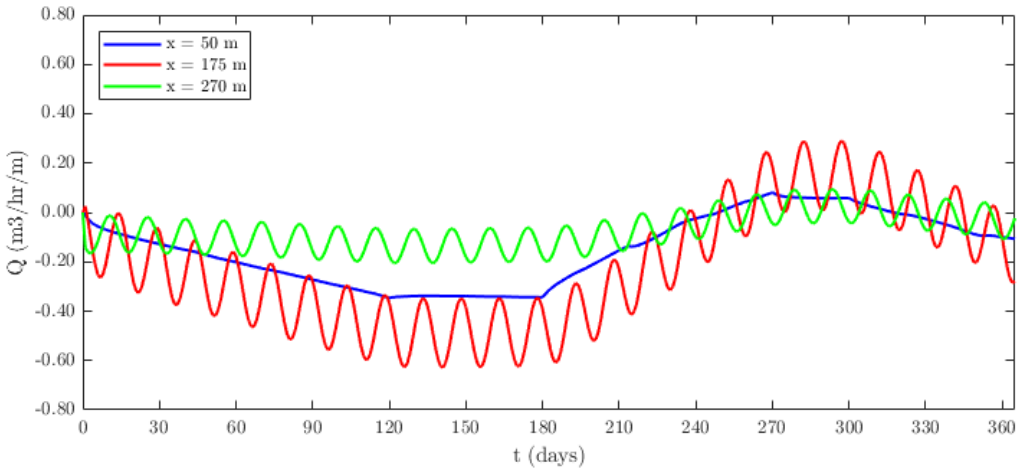

Fig. 39 Annual variation of flow quantity across various cross-sections of -20 m section with α_l = 30 m, α_t = 3 m

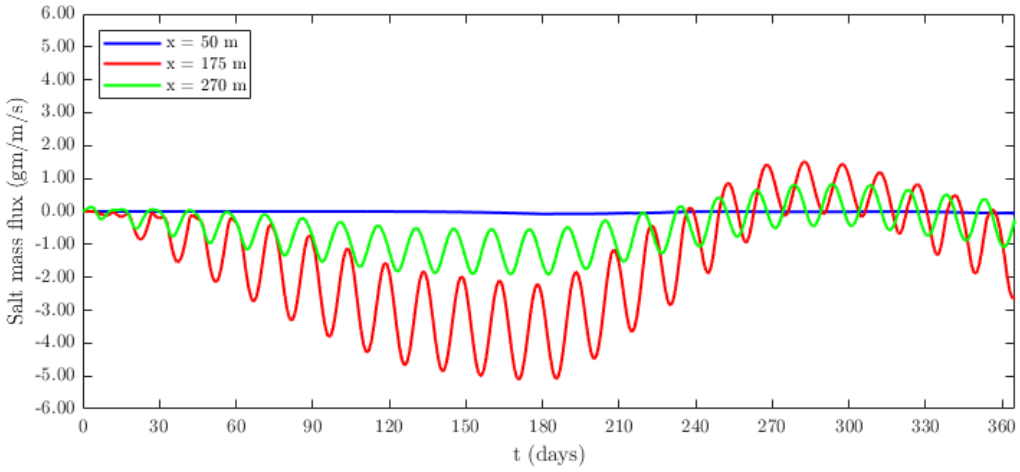

Fig. 40 Annual variation of salt mass flux across various cross-sections of -20 m section with α_l = 30 m, α_t = 3 m

5.2.5 -10 m section

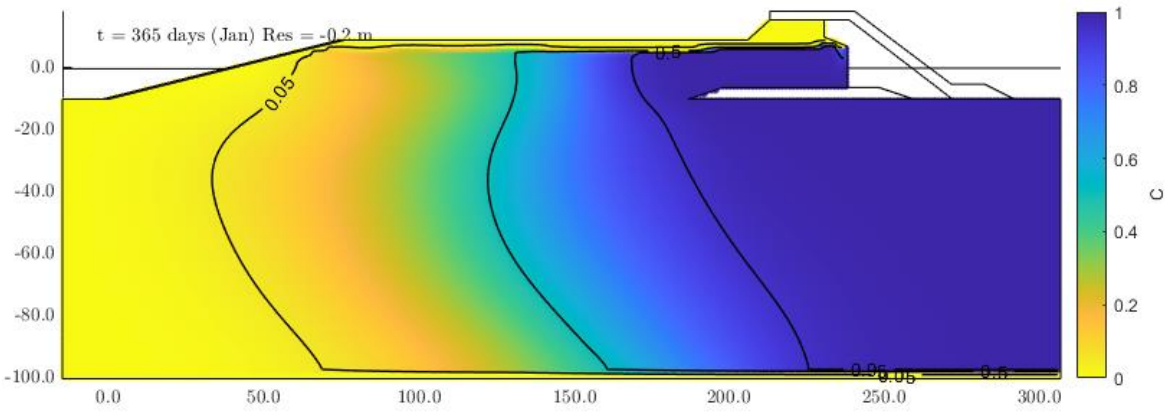

Fig. 41 Normalized salt mass fraction at 1 year for -10 m section (with caisson) with α_l = 30 m, α_t = 3 m

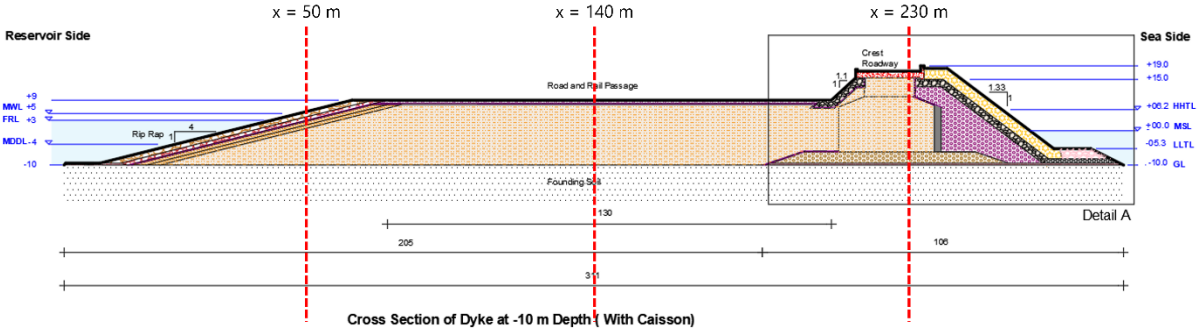

Fig. 42 Cross-sections along the -10 m embankment section (with caisson)

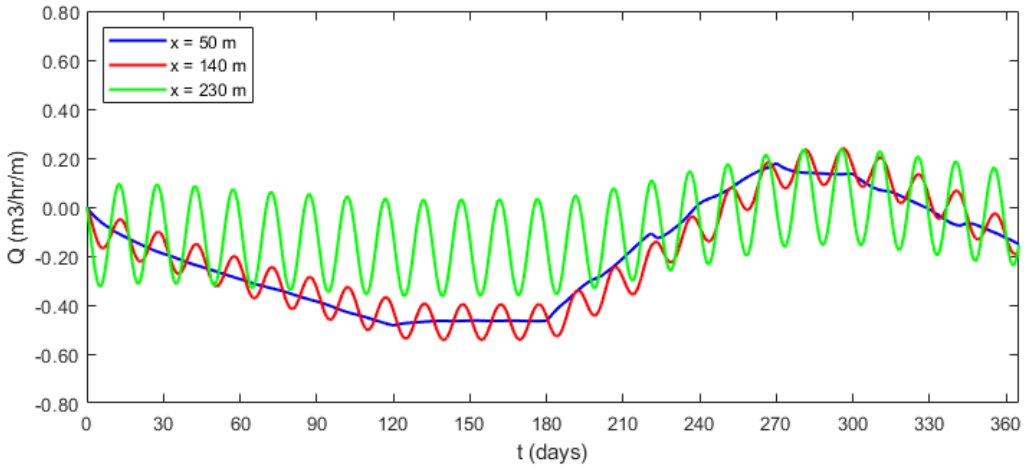

Fig. 43 Annual variation of flow quantity across various cross-sections of -10 m section (with caisson) with α_l = 30 m, α_t = 3 m

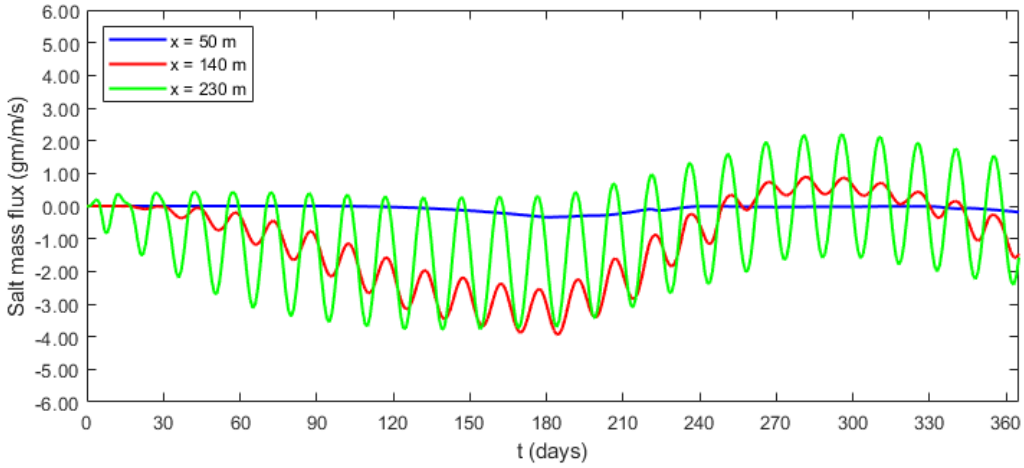

Fig. 44 Annual variation of salt mass flux across various cross-sections of -10 m section (with caisson) with α_l = 30 m, α_t = 3 m

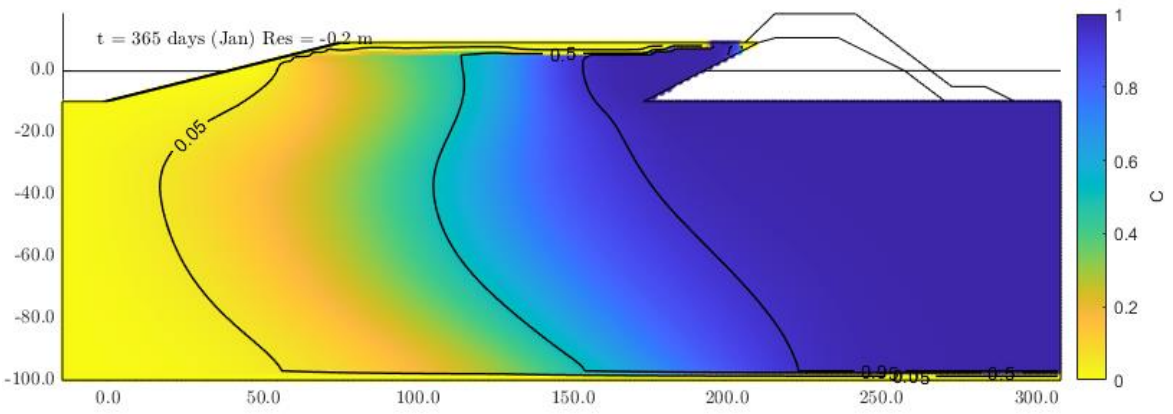

Fig. 45 Normalized salt mass fraction at 1 year for -10 m section (without caisson) with α_l = 30 m, α_t = 3 m

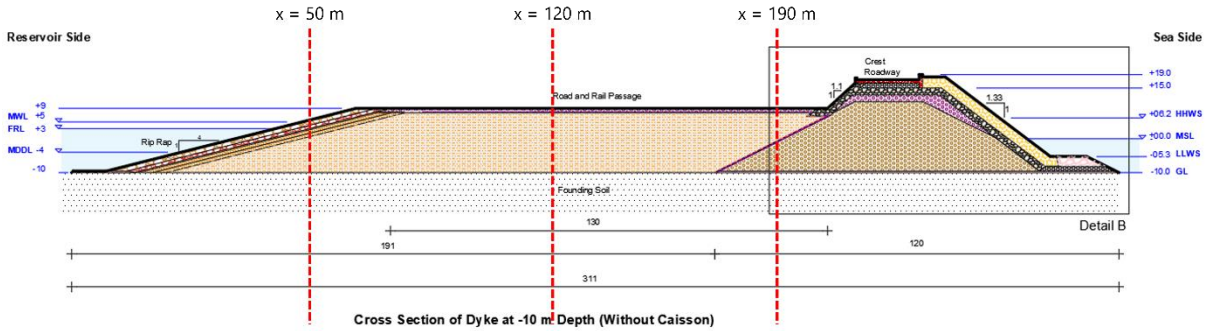

Fig. 46 Cross-sections along the -10 m embankment section (without caisson)

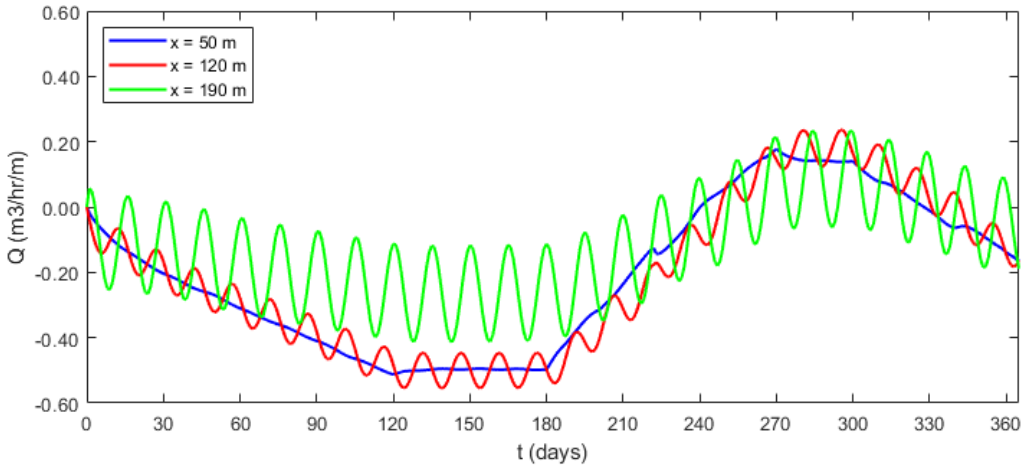

Fig. 47 Annual variation of flow quantity across various cross-sections of -10 m section (without caisson) with α_l = 30 m, α_t = 3 m

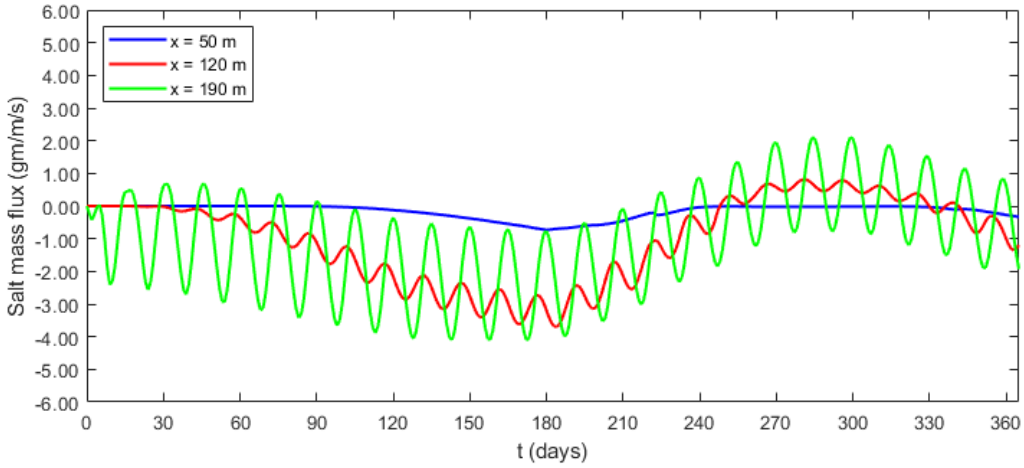

Fig. 48 Annual variation of salt mass flux across various cross-sections of -10 m section (without caisson) with α_l = 30 m, α_t = 3 m

5.2.6 0 m section

For sections at 0 m, +2 m, and +5 m, the foundation consists primarily of clay with layers of sand. Based on the marine geotechnical investigation reported provided by NCCR, the soil profile upto 100 m consists of approximately 20 to 25 m of sand (in several layers), while the remaining is clay. To provide a conservative estimate of the flow and salt transport quantities, the permeability of the foundation in these regions is estimated as a weighted average of the permeability of the seabed sand and clay, i.e., k = (6.5 × 10^{-5} m/s) × 0.2 + (4.3 × 10^{-7} m/s) × 0.8 ≈ **1.3 × 10^{-5} m/s.**

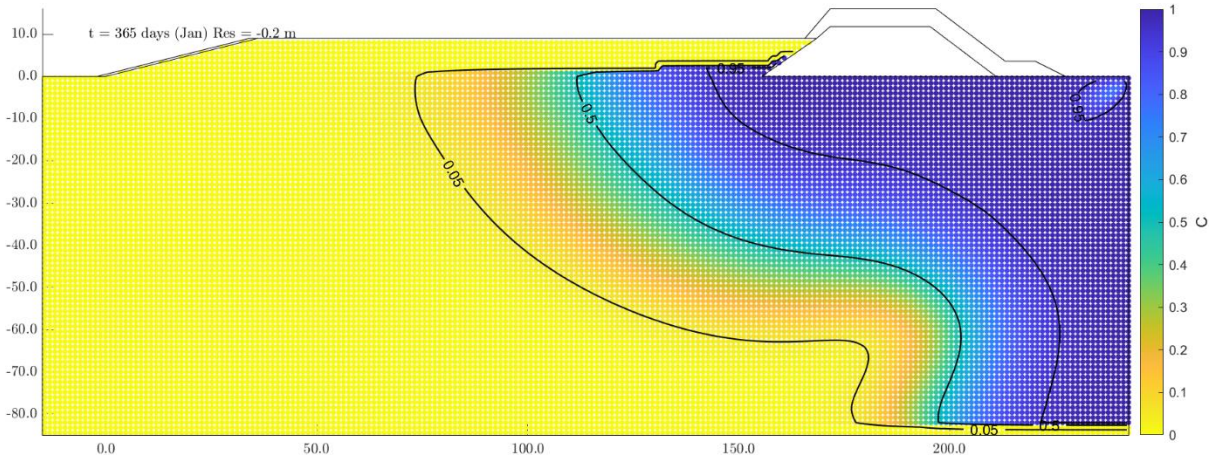

Fig. 49 Normalized salt mass fraction at 1 year for 0 m section with α_l = 20 m, α_t = 2 m

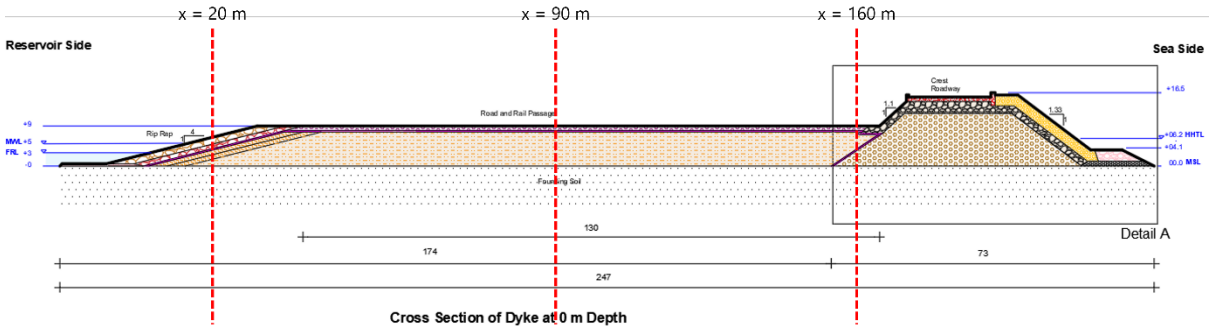

Fig. 50 Cross-sections along the 0 m embankment section

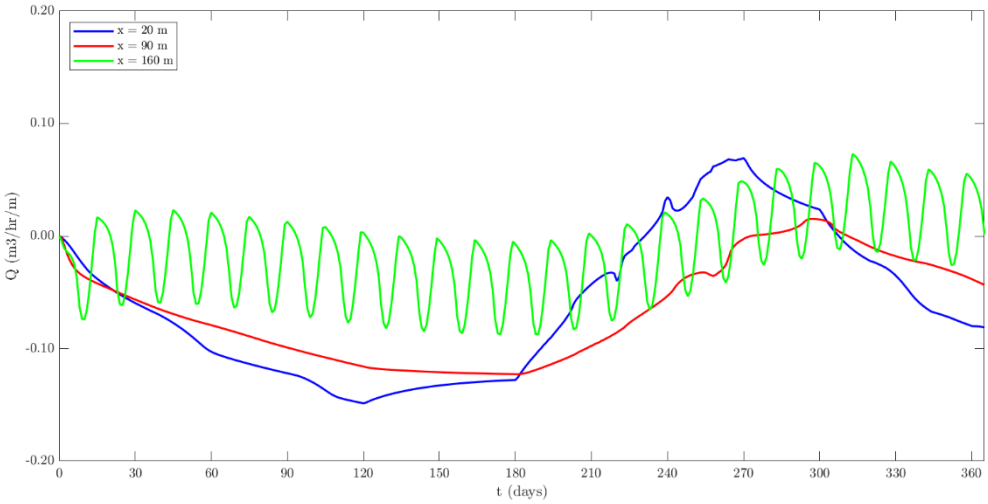

Fig. 51 Annual variation of flow quantity across various cross-sections of 0 m section with α_l = 20 m, α_t = 2 m

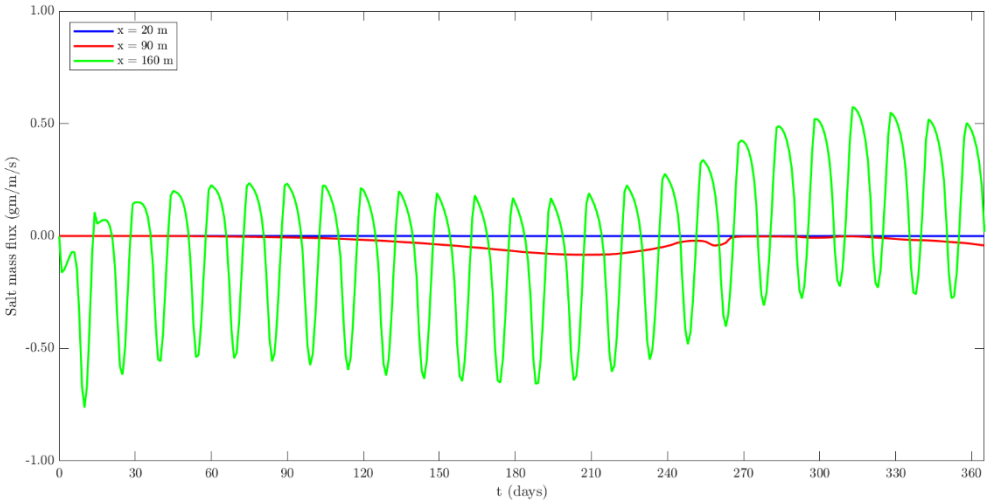

Fig. 52 Annual variation of salt mass flux across various cross-sections of 0 m section with α_l = 20 m, α_t = 2 m

5.2.7 +2 m section

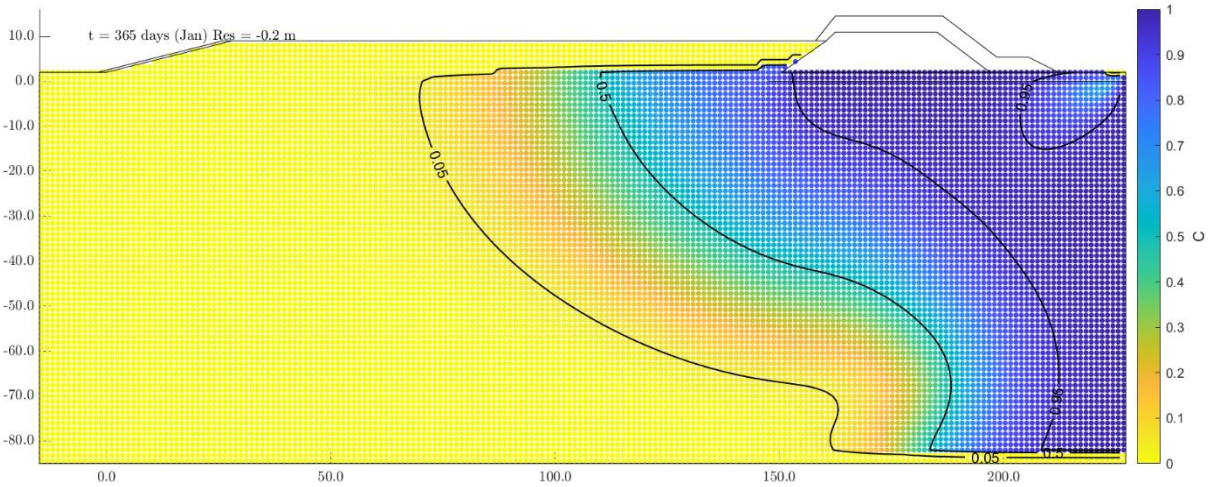

Fig. 53 Normalized salt mass fraction at 1 year for +2 m section with α_l = 20 m, α_t = 2 m

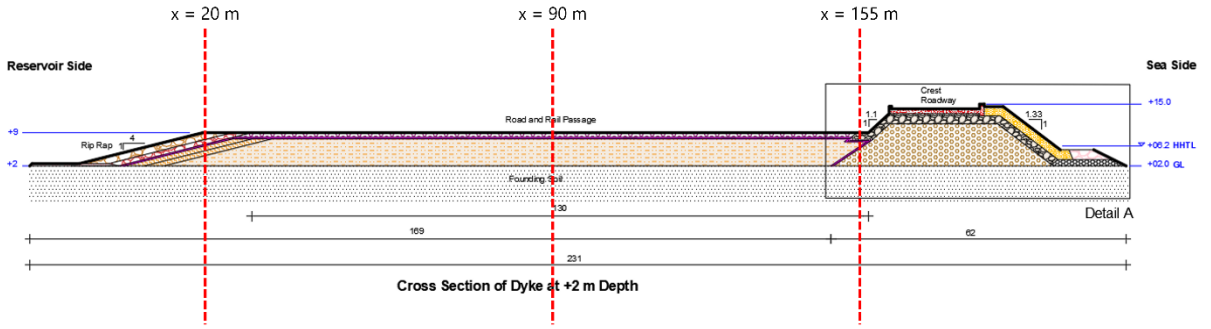

Fig. 54 Cross-sections along the +2 m embankment section

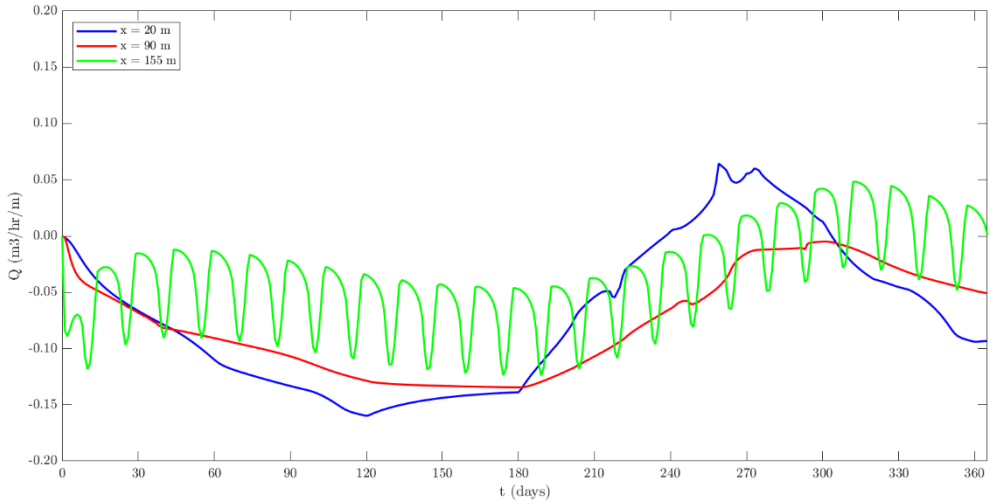

Fig. 55 Annual variation of flow quantity across various cross-sections of +2 m section with α_l = 20 m, α_t = 2 m

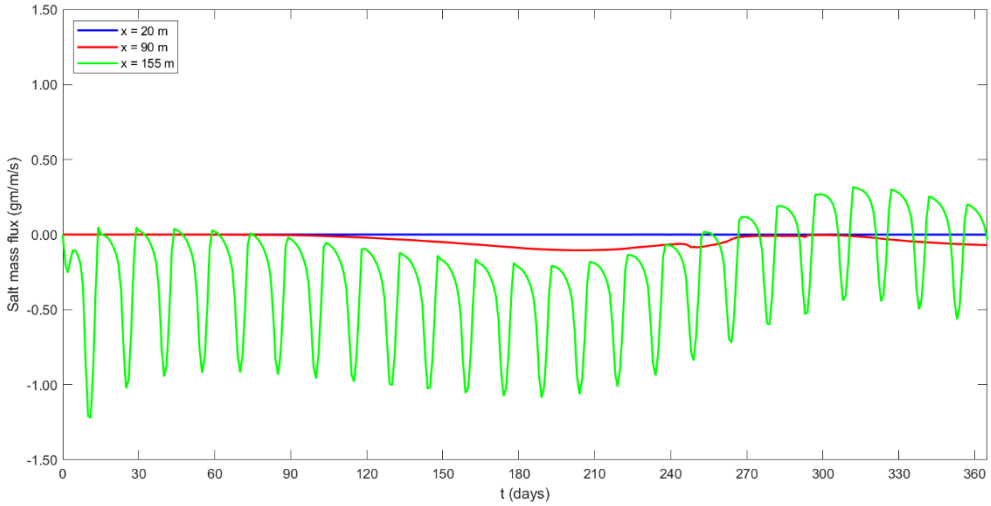

Fig. 56 Annual variation of salt mass flux across various cross-sections of +2 m section with α_l = 20 m, α_t = 2 m

5.2.8 +5 m section

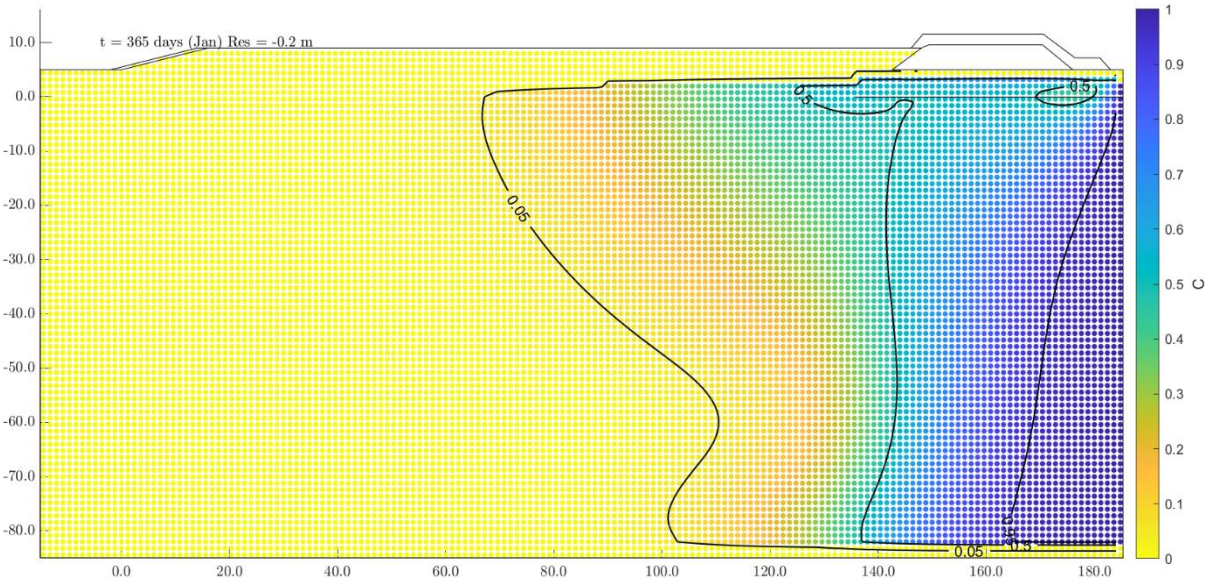

Fig. 57 Normalized salt mass fraction at 1 year for +5 m section with α_l = 20 m, α_t = 2 m

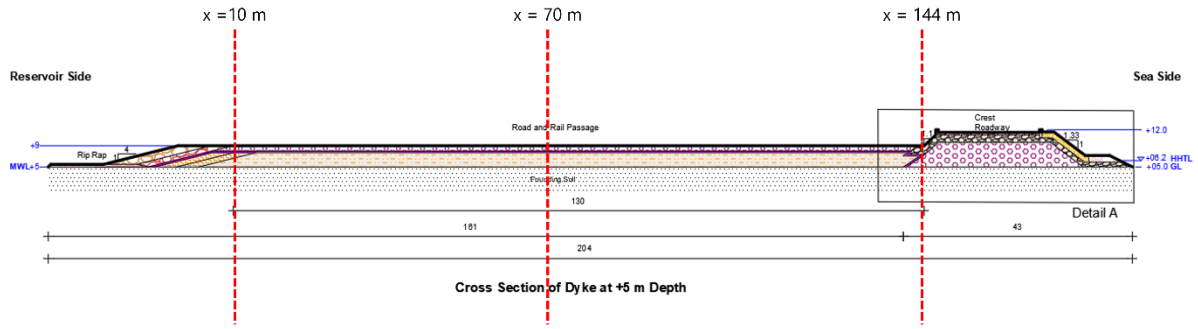

Fig. 58 Cross-sections along the +5 m embankment section

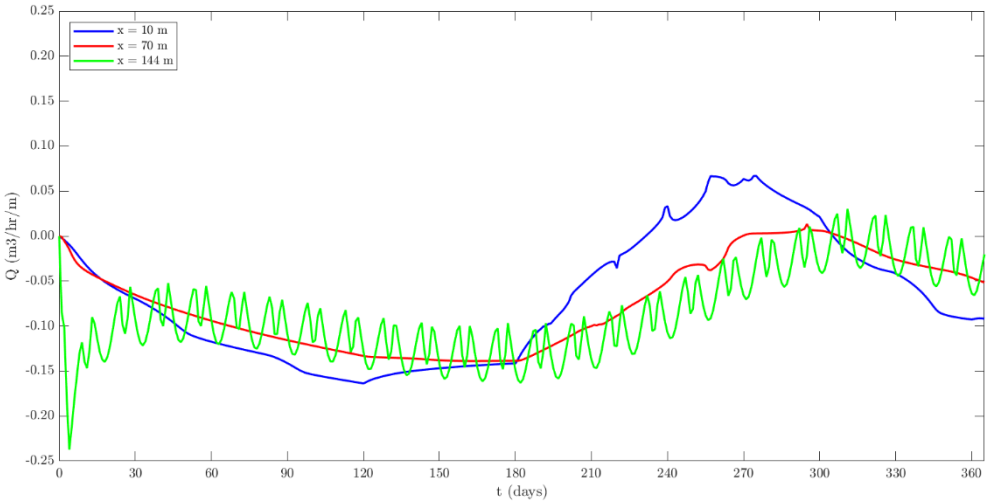

Fig. 59 Annual variation of flow quantity across various cross-sections of +5 m section with α_l = 20 m, α_t = 2 m

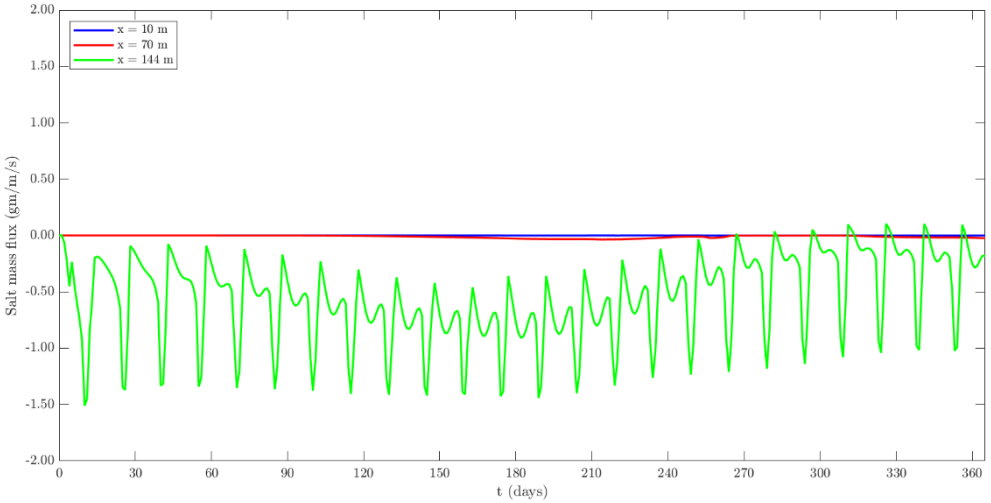

Fig. 60 Annual variation of salt mass flux across various cross-sections of +5 m section with α_l = 20 m, α_t = 2 m

5.2.9 Flood regulator

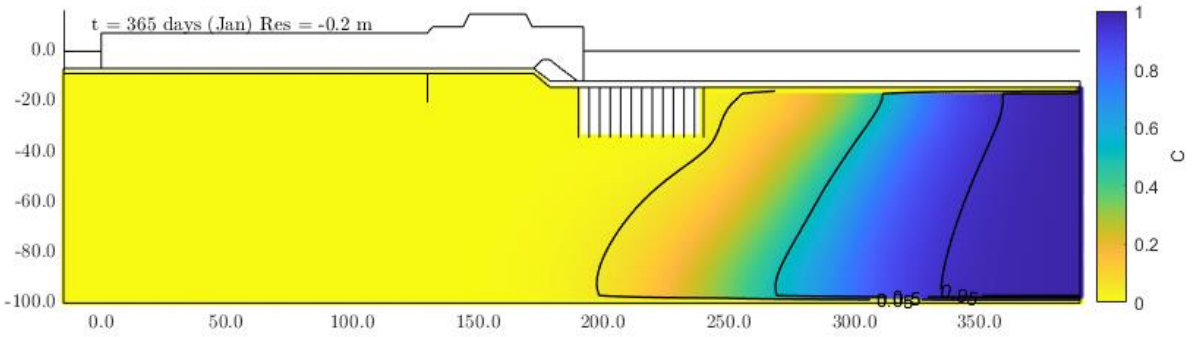

Fig. 61 Normalized salt mass fraction at 1 year for flood regulator section with α_l = 30 m, α_t = 3 m

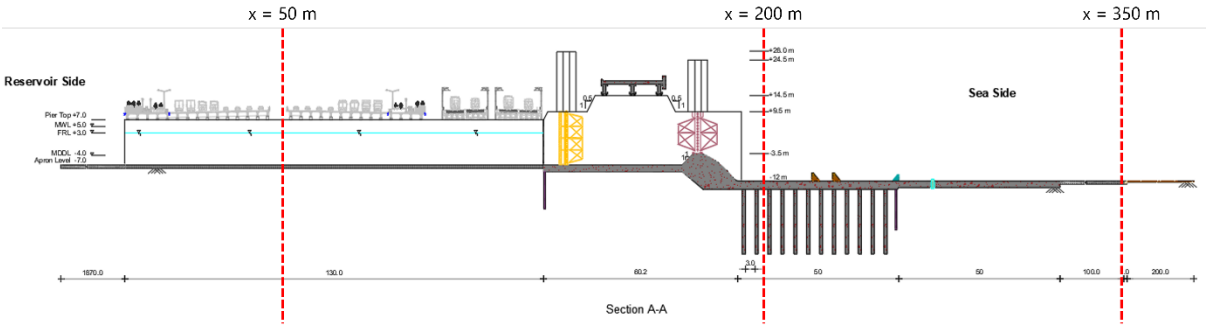

Fig. 62 Cross-sections along the flood regulator section

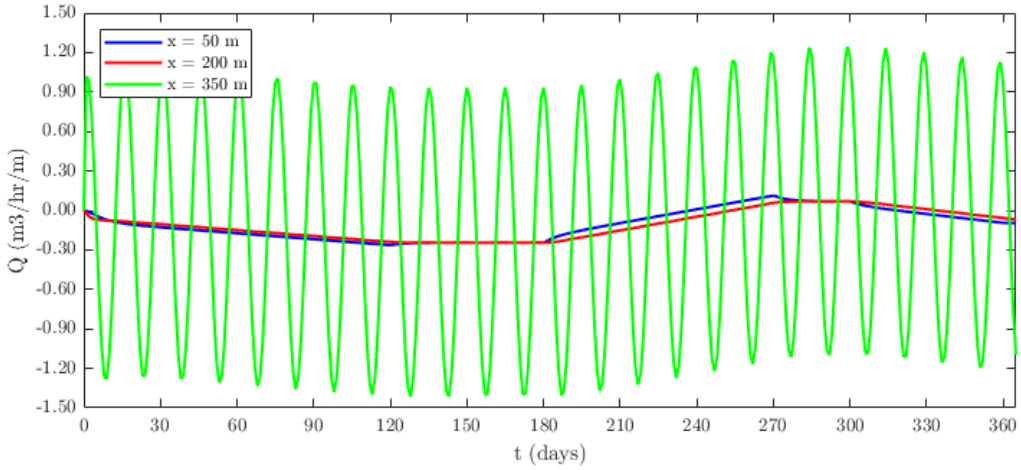

Fig. 63 Annual variation of flow quantity across various cross-sections of flood regulator section with α_l = 30 m, α_t = 3 m

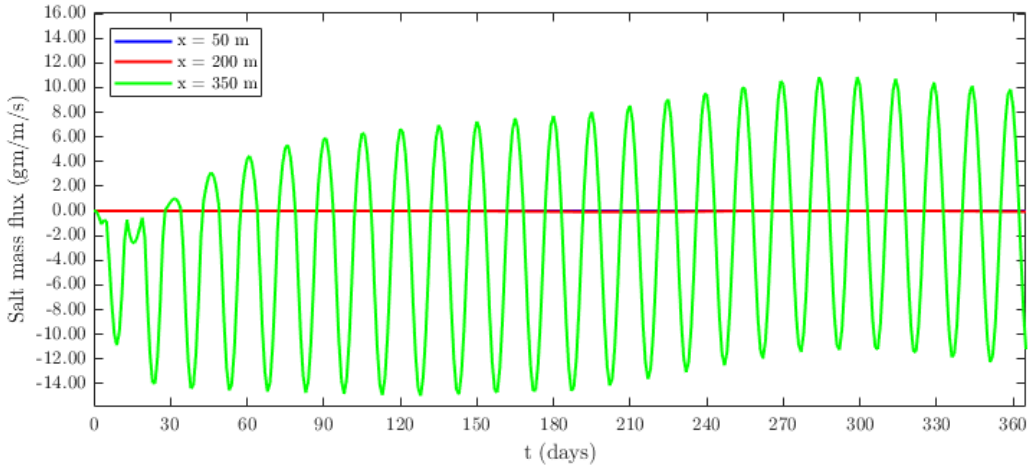

Fig. 64 Annual variation of salt mass flux across various cross-sections of flood regulator section with α_l = 30 m, α_t = 3 m

The total quantity of water flowing through the embankment and foundation in 1 year for the various cross-sections is shown in Tables 6 to 16.

Table 6 Total quantity of water (m^3/m) flowing through embankment and foundation in 1 year at -30 m section

Section	Through embankment	Through foundation
x = 75 m	-113	-1586
x = 175 m	-231	-2446
x = 310 m	-719	-571

Table 7 Total quantity of water (m^3/m) flowing through embankment and foundation in 1 year at -25 m section

Section	Through embankment	Through foundation
x = 50 m	-62	-1242
x = 175 m	-152	-2170
x = 295 m	-1007	-563

Table 8 Total quantity of water (m^3/m) flowing through embankment and foundation in 1 year at -20 m section

Section	Through embankment	Through foundation
x = 50 m	-86	-1293
x = 175 m	-88	-1896
x = 270 m	-744	-637

Table 9 Total quantity of water (m^3/m) flowing through embankment and foundation in 1 year at -15 m section

Section	Through embankment	Through foundation
x = 50 m	-260	-1542
x = 150 m	-37	-1729
x = 250 m	0	-592

Table 10 Total quantity of water (m^3/m) flowing through embankment and foundation in 1 year at -10 m (with caisson) section

Section	Through embankment	Through foundation
x = 50 m	-87	-1656
x = 140 m	-15	-1720
x = 230 m	-504	-772

Table 11 Total quantity of water (m^3/m) flowing through embankment and foundation in 1 year at -10 m (without caisson) section

Section	Through embankment	Through foundation
x = 50 m	-77	-1786
x = 120 m	-28	-1811
x = 190 m	-209	-1044

Table 12 Total quantity of water (m^3/m) flowing through embankment and foundation in 1 year at -5 m section

Section	Through embankment	Through foundation
x = 25 m	-45	-1841
x = 100 m	-16	-1784
x = 175 m	-230	-925

Table 13 Total quantity of water (m^3/m) flowing through embankment and foundation in 1 year at 0 m section

Section	Through embankment	Through foundation
x = 20 m	0	-527
x = 90 m	0	-574
x = 160 m	-62	-88

Table 14 Total quantity of water (m^3/m) flowing through embankment and foundation in 1 year at +2 m section

Section	Through embankment	Through foundation
x = 20 m	0	-611
x = 90 m	0	-677
x = 155 m	-3	-312

Table 15 Total quantity of water (m^3/m) flowing through embankment and foundation in 1 year at +5 m section

Section	Through embankment	Through foundation
x = 10 m	0	-603
x = 70 m	0	-650
x = 144 m	0	-752

Table 16 Total quantity of water (m^3/m) flowing through embankment and foundation in 1 year at flood regulator section

Section	Through embankment	Through foundation
x = 50 m	NA	-930
x = 200 m	NA	-941
x = 350 m	NA	-920

The cumulative salt mass flux through the embankment and foundation in 1 year for the various cross-sections is shown in Tables 17 to 27.

Table 17 Total quantity of salt mass (kg/m) transported through embankment and foundation in 1 year at -30 m section

Section	Through embankment	Through foundation
x = 75 m	-201	-1326
x = 175 m	-10788	-44918
x = 310 m	-25233	-10784

Table 18 Total quantity of salt mass (kg/m) transported through embankment and foundation in 1 year at -25 m section

Section	Through embankment	Through foundation
x = 50 m	-35	-356
x = 175 m	-9338	-44750
x = 295 m	-14388	-12208

Table 19 Total quantity of salt mass (kg/m) transported through embankment and foundation in 1 year at -20 m section

Section	Through embankment	Through foundation
x = 50 m	-85	-570
x = 175 m	-7448	-44378
x = 270 m	-25828	-16299

Table 20 Total quantity of salt mass (kg/m) transported through embankment and foundation in 1 year at -15 m section

Section	Through embankment	Through foundation
x = 50 m	-329	-2100
x = 150 m	-2830	-40500
x = 250 m	0	-23700

Table 21 Total quantity of salt mass (kg/m) transported through embankment and foundation in 1 year at -10 m (with caisson) section

Section	Through embankment	Through foundation
x = 50 m	-313	-2335
x = 140 m	-1946	-33348
x = 230 m	-17490	-25517

Table 22 Total quantity of salt mass (kg/m) transported through embankment and foundation in 1 year at -10 m (without caisson) section

Section	Through embankment	Through foundation
x = 50 m	-635	-4980
x = 120 m	-1820	-31260
x = 190 m	-7475	-31444

Table 23 Total quantity of salt mass (kg/m) transported through embankment and foundation in 1 year at -5 m section

Section	Through embankment	Through foundation
x = 25 m	-139	-3206
x = 100 m	-524	-25491
x = 175 m	-6311	-33738

Table 24 Total quantity of salt mass (kg/m) transported through embankment and foundation in 1 year at 0 m section

Section	Through embankment	Through foundation
x = 20 m	-0.2	-0.9
x = 90 m	-26	-786
x = 160 m	-62	-705

Table 25 Total quantity of salt mass (kg/m) transported through embankment and foundation in 1 year at +2 m section

Section	Through embankment	Through foundation
x = 20 m	0	-1.2
x = 90 m	-0.5	-1171
x = 155 m	0	-8140

Table 26 Total quantity of salt mass (kg/m) transported through embankment and foundation in 1 year at +5 m section

Section	Through embankment	Through foundation
x = 10 m	0	-0.6
x = 70 m	0	-326
x = 144 m	0	-17252

Table 27 Total quantity of salt mass (kg/m) transported through embankment and foundation in 1 year at flood regulator section

Section	Through embankment	Through foundation
x = 50 m	NA	0
x = 200 m	NA	-558
x = 350 m	NA	-72286

6. Summary

Quantity of seepage and salt mass influx were given in Tables 2 to 27 for varying conditions as per the scope of the work.

December 2023 (G. V. Ramana)

References

[1] Bear J, Cheng AH-D. Modeling groundwater flow and contaminant transport. vol. 23. Springer; 2010. https://doi.org/https://doi.org/10.1007/978-1-4020-6682-5.

[2] Gingold RA, Monaghan JJ. Smoothed particle hydrodynamics: theory and application to non-spherical stars. Mon Not R Astron Soc 1977;181:375–89. https://doi.org/10.1093/mnras/181.3.375.

[3] Bui HH, Nguyen GD. Smoothed particle hydrodynamics (SPH) and its applications in geomechanics: From solid fracture to granular behaviour and multiphase flows in porous media. Comput Geotech 2021;138:104315. https://doi.org/10.1016/j.compgeo.2021.104315.

[4] Lian Y, Bui HH, Nguyen GD, Tran HT, Haque A. A general SPH framework for transient seepage flows through unsaturated porous media considering anisotropic diffusion. Comput Methods Appl Mech Eng 2021;387:114169. https://doi.org/10.1016/j.cma.2021.114169.

[5] PLAXIS (2019) PLAXIS 2D Reference Manual. Bentley Systems International Limited, Dublin. n.d.

[6] Fetter CW, Boving T, Kreamer D. Contaminant hydrogeology. Waveland Press; 2017.

[7] Booker JR, Quigley RM, Rowe RK. Clayey barrier systems for waste disposal facilities. CRC Press; 1997.